1994

The Reduction Of Concentration Values In A Contaminant Cloud In Environmental Flows

William Kenneth Heagy

THE REDUCTION OF CONCENTRATION VALUES IN A CONTAMINANT CLOUD IN ENVIRONMENTAL FLOWS

By
William K. Heagy

Department of Applied Mathematics

Submitted in partial fulfilment
of the requirements for the degree of
Doctor of Philosophy

Faculty of Graduate Studies
The University of Western Ontario
London, Ontario
July, 1994

National Library
of Canada

Acquisitions and
Bibliographic Services Branch

395 Wellington Street
Ottawa, Ontario
K1A 0N4

Bibliothèque nationale
du Canada

Direction des acquisitions et
des services bibliographiques

395, rue Wellington
Ottawa (Ontario)
K1A 0N4

Your file Votre référence

Our file Notre référence

ISBN 0-315-93196-5

Canada

Abstract

This thesis considers the spread of contaminant after the release of a cloud of toxic gas into the atmosphere. A new measure, the *Expected Mass Fraction* (EMF), presents an improvement over the mean dosage as an indicator of the risk associated with the cloud release. The study shows that the variability of estimates of the EMF should be comparable to that of the dosage, so that reliable evaluation should be possible in many situations. The theory is based on the Chatwin-Sullivan α-β formulation, which relates the mean concentration to the moments of the probability density function of the concentration. The proposed new measure is validated with data from a wind tunnel study performed at the Warren Spring Laboratory in Great Britain. The thesis concludes with an extension of the theory to incorporate G.K. Batchelor's analysis of the rate of growth of a cloud released at the earth's surface into the atmospheric boundary layer. These results should have application in the analysis of risk from accidental release of toxic gases into the atmosphere. By extending the information available to include predictions of concentrations of contaminant, the analysis can assist in analyzing other problems such as flammability. The same methodology should also find application in dissipation problems in other turbulent flows, such as lakes, rivers or oceans.

Acknowledgements

I wish to thank first my advisor, Professor Paul J. Sullivan for his excellent guidance and support. Thanks go also to Dr. David Hall of the Warren Spring Laboratory, Great Britain, for providing the data used to validate the theory presented in this thesis. Finally I thank the many other friends and associates who have helped me to complete this thesis.

Contents

List of Tables

List of Figures

Nomenclature

C average concentration in Chatwin-Sullivan theory

$C_0(t)$ reference concentration in Chatwin-Sullivan theory

D turbulent diffusivity parameter in example

$d(\mathbf{x})$ dosage, a random variable

d'_k dose associated with $\Gamma'_{k,i}$

$E(l)$ probable length of strand within cylinder

EMF expected mass fraction

g acceleration due to gravity

$H(\theta)$ Heaviside step function

k kurtosis

L, U length and velocity scales for definition of Richardson number

L_0 distance from release point to virtual origin in Subsection 4.4.1

l length of strand within cylinder

$M_n(\mathbf{x},t)$ n^{th} moment of $p(\theta;\mathbf{x},t)$

$M'_n(\mathbf{x})$ time integral of $M_n(\mathbf{x},t)$

$\hat{M}_n(\mathbf{x})$ n^{th} moment of $\hat{p}(\mathbf{x})$

$m_n(\mathbf{x}, t)$ n^{th} central moment of $p(\theta; \mathbf{x}, t)$

N expected number of sample points in box

N_{trials} number of releases in an experiment

$p(\theta; \mathbf{x}, t)\, d\theta$ prob$\{\theta \leq \Gamma(\mathbf{x}, t) < \theta + d\theta\}$

$p'(\theta; \mathbf{x})$ expected time of residence

$\hat{p}(\theta; \mathbf{x})$ expected mass fraction

$\hat{p}_n(\theta_n)$ expected mass fraction normalized according to Batchelor hypothesis in Subsection 4.4.1

$\hat{p}_A(\mathbf{x})$ $\hat{p}(\mathbf{x})$ when measured by a probe averaging over area A

Q total mass of contaminant released

Q_i mass of contaminant in i^{th} sample

R, r radius

Ri bulk Richardson number

s skewness

t time after release

t_R reference time for normalization

t_X time offset for normalization

t_n time after release adjusted by virtual time offset

u reference speed

$\mathbf{u}(\mathbf{x}, t)$ instantaneous wind speed at point $\mathbf{x}$ and time t

V volume (region in space)

WSL Warren Spring Laboratory

x, y, z spatial coordinates

x_P probe position for normalization

x_n normalized length coordinate in Batchelor normalization in Subsection 4.4.1

z_0 roughness length parameter in logarithmic wind speed profile

α angle of strand to reference plane

$\alpha(t)$, $\beta(t)$ parameters in the Chatwin-Sullivan formulation

$\Gamma(\mathbf{x}, t)$ concentration, a random variable, normalized by θ_0

δA effective sampling area of probe

δt length of time for one sample

ϵ total rate of viscous dissipation of kinetic energy per unit mass

θ contaminant or tracer concentration value

θ_0 initial concentration

θ_n normalized concentration using Batchelor hypothesis in Subsection 4.4.1

$\theta_{1/2}$ median concentration

$\theta'_{k,i}$ i^{th} observed concentration reading in k^{th} release

θ_t background threshold concentration in Moseley closure formulation

κ coefficient of molecular diffusion

λ conduction cut-off length

ν kinematic viscosity

ρ mass of contaminant per unit length along strand

ρ_{gas} density of released fluid

ρ_{air} density of ambient air

$\sigma(t)$ length scale in example

χ normalized concentration in Chatwin-Sullivan formulation formulation

$\overline{\cdot}$ ensemble average

Chapter 1

Introduction

Environmental dispersion deals with the spreading out of toxic or otherwise dangerous materials to an acceptable level or to a level at which natural processes can dispose of them. For instance, the wind spreads the emissions from automobiles until photo-synthesis converts most of the carbon dioxide in the emissions back into carbohydrates. Similarly other processes eventually convert the other ingredients, such as nitrous oxides and carbon monoxide, into less harmful products. The spreading out in the atmosphere by turbulent mixing processes, to the point where molecular diffusion can actually dilute the high concentrations of contaminant, quickly reduces the initially lethal concentrations coming out of the exhaust pipe to manageable levels.

Smoke rises from a campfire, wandering back and forth as the gusts of wind carry the smoke in different directions. Close to the ground the smoke moves slowly, sheltered from the wind by surrounding trees and bushes. Or the smoke rises higher and gets carried briskly away by the breeze. On some calm days it just gathers in a dense choking cloud around the fire.

Two characteristics of this behavior motivate the present study. First, the pattern of smoke dispersal changes continually, both in direction and concentration. Second, at least with smoke, people notice long exposure more than short exposure, and high

concentration more than low concentration. No matter where a person sits, sooner or later the smoke will find him. A little bit of smoke people tolerate, but extended periods of thick smoke cause them to move. This thesis studies the variability of airborne tracers such as smoke, both the variability of the tracer's convection and the effects of the tracer's spatial distribution on the averaging process inevitably involved in its perception, by instrumentation or by people.

Consider the process of trying to predict the exposure of people to smoke from a campfire. At any given time, the smoke will miss some of them completely, while others will receive smoke of varying concentrations. Much of the time, no one will suffer from the highest concentration of smoke around the fire. The highest concentration will occur only in a small volume, which will occur almost anywhere at some time, but only rarely at a given location. To establish the statistics of the highest concentrations requires either long term observations to give confidence of observing the highest concentrations and estimating their frequency of occurrence, or else requires very many observers to ensure that someone will observe the highest concentration at any given time. In either case, most of the time most of the people will not see much happening.

The release of a cloud of contaminant near the earth's surface can create many dangers which need evaluation and quantification, to say nothing of response with appropriate measures. This chapter introduces the problem of dispersion of clouds or plumes of contaminant gases or smoke, in the context of risk assessment and hazard evaluation.

The problem has two phases. First, existing data require analysis and evaluation, to provide a database of relevant parameters and to provide guidance for future research. Second, reaction to a specific situation requires a model which can give quantitative information about the danger posed, and the best remedial action possible. This requires dealing with incomplete information and uncertainty at many levels,

from the large scale "What happened?" down to the level of molecular diffusion at scales of a fraction of a centimeter.

This study establishes a relationship between concentrations which observers see most of the time, the typical behavior, and the highest concentrations, which have greater importance, but which happen rarely. If these events happened more frequently, then they would not represent the "unusual", but rather the norm. While the norm may still represent a problem, it does not require a great statistical effort to analyze. People recognize a frequently occurring danger and can deal with it, avoid it or cure it. The trouble comes when hazards arise infrequently. The rare event requires more effort to establish appropriate measures. Precautions have to be evaluated. Do people need to take precautions? Some recommended precautions cause more danger than the problem they are intended to cure, as in the case of an accidental release of toxic gas (discussed in Chapter 5) where recommended emergency measures moved people *into* more hazaradous areas. Dispersion problems require assessing the dangers so that people can decide whether to accept the risks or cure the problem, or possibly even decide that no problem exists, or that no significant danger occurs. For instance, the situation may not lead to dangerous concentrations. The carbon dioxide normally in the air occurs only at low concentrations and causes no concern, even though high concentrations of carbon dioxide can kill. Indeed, the breathing mechanism requires low concentrations to keep it operating properly. If the carbon dioxide level in the blood gets too low, the body may stop breathing, because it looks at the carbon dioxide level rather than the oxygen level to determine how much it needs to breath. If the carbon dioxide level gets too low, the body decides it can stop breathing. So the body requires a minimum level of carbon dioxide for health. This illustrates one frequent aspect of dispersion problems. Biologically, data for high concentrations for short times does not apply to low concentrations for long times. In the case of carbon dioxide, long exposure to low concentrations benefits the body, while short exposure

to high concentration can kill. To deal with many of these problems requires knowing both the concentration and duration of exposure.

Another aspect comes from the ability of the body to recover. Intermittent short exposure to high concentrations, with recovery time in between, may not cause any danger. But if the same exposure comes over too short a time interval, with not enough recovery time, harm may result. Evaluation requires knowing much about both the statistics of the contaminant and the way that the body reacts to it, at high or low concentrations, for long or short times, with frequent or infrequent exposure.

The distribution of concentration in time and in space requires consideration. Breathing may average out very small volumes of very high concentrations, to produce larger volumes of tolerable concentrations. Similarly, many points of high concentration close together might, even when averaged, produce a dangerous effect, while the same points, spread out more, would produce no harm.

When considering a "real" event, the importance of the event depends not just on the processes involved, but on the probability of the event happening. For instance, looking at an accident such as the Mississauga train derailment in 1981, first the chance of the derailment and a spill happening needs evaluating. This thesis considers the next step in the analysis, the conditional probability of "Given such a spill, who does it put at risk, how much danger does it cause, ...?" The study looks at the various probabilities in the outcome, such as mixing and convection processes, concentration or dilution, and large or multiple doses. The relationship between toxicity, concentration and duration forms the next step in the sequence of analysis starting with analysis of the probability of an accident happening and proceeding through the statistics of the physical processes of cloud spread in the current study. The results of the present study should prove of value to toxicological studies such as those of Griffiths [Gri91]. More general risk evaluation procedures, which include evaluation of the event happening and the severity of the consequences, in a context

that also includes costs of alternatives allowing rational determination of options, can then incorporate this analysis.

1.1 Physics of the Problem

The fluid flows which drive atmospheric mixing problems have very large length scales, developing over many kilometers, and moderate velocities, of the order of 10m/s. The Reynolds Number based on such dimensions typically has a magnitude greater than 10^6. Consequently atmospheric flows almost always involve turbulence, and the flow near the earth's surface forms a turbulent boundary layer. A lack of predictability characterizes turbulence. Dealing with it requires dealing with random variables, quantities specified only by statistical measures. Predictions deal with probable outcomes, not deterministic calculations.

A transport equation describes the diffusion of a passive contaminant in a turbulent flow:

$$\frac{\partial \overline{\Gamma}}{\partial t} + \nabla \cdot \overline{\mathbf{u}\Gamma} = \kappa \nabla^2 \overline{\Gamma}. \tag{1}$$

This equation comes directly from the equation for the transport of a passive scalar in an incompressible fluid flow (see e.g [TL72, Chapter 2]). The tracer moves with the fluid, and the change in concentration at a point comes only from convection (the left hand side of equation (1)) or diffusion (the right hand side of equation (1)), with no tracer created or destroyed. The concentration of contaminant, Γ, depends on position and time, as does the velocity field $\mathbf{u}$. The over-bar, $\overline{\cdot}$, denotes the ensemble average. The mean concentration, $\overline{\Gamma}$, appears as a linear term in the equation. However, the unknown term $\nabla \cdot \overline{\mathbf{u}\Gamma}$ characterizes the turbulence closure problem, coming from the average of the product of two factors. With no *a priori* justification for any closure hypothesis or formula to describe this term, thorough experiments must validate any closure hypothesis or other semi-empirical theory [Cha90].

The model studied here starts with the release of a "blob" of contaminant into a turbulent flow. The blob initially has uniform concentration θ_0. Turbulent convective motions stretch out the contaminant into ever thinning sheets and strands until thickening due to diffusion balances the thinning due to turbulent strain. This balance happens at lengths of the order of the conduction cut-off length

$$\lambda = (\nu\kappa^2/\epsilon)^{1/4} \tag{2}$$

of order 10^{-4}–10^{-5}m in most flows [CS79]. Here, κ represents the coefficient of molecular diffusion, ν is the kinematic viscosity and ϵ measures the total rate of viscous dissipation of kinetic energy per unit mass. The conduction cut-off length λ represents the length scale at which molecular diffusion, spreading out the tracer, balances the reduction of the thickness of strands of tracer from the strain caused by the fluid's turbulent motion. Not until the strains have reduced the thickness to this order will the relatively slow-acting molecular diffusion begin to counteract the turbulent strains, which are limited by the fluid viscosity at these short length scales. Experiments using litmus fluids in a contaminant jet show virtually *all* contaminant above a given threshold value resides in sheets and strands of thickness λ [BC92]. Dahm *et al* [DSB91] resolved a cube within a contaminant jet and showed the same inhomogeneity and small-scale structure. Such studies show that the *only* molecular mixing between host and contaminant fluid comes from molecular diffusion κ acting on the λ scale. In the non-physical case of $\kappa = 0$ for example, if the initial release has uniform concentration θ_0, then the contaminant concentration $\Gamma(\mathbf{x}, t)$ at the position located by vector $\mathbf{x}$ at time t will always have values of either θ_0 or zero.

1.2 Ensemble Average Values

The random variable $\Gamma(\mathbf{x}, t)$ is the instantaneous point value of the contaminant concentration. For the case of a cloud, one must have repeated trials to establish parameters, unlike continuous sources for which conventional studies use time averages, with appeal to the ergodic theorem. Even in an ideal steady, isotropic turbulent field, for a cloud, $\Gamma(\mathbf{x}, t)$ represents an intrinsically non-homogeneous, non-stationary random variable. Environmental flows themselves generally have unsteady and inhomogeneous properties. Normally applications require (at least) the one-point probability density function

$$p(\theta; \mathbf{x}, t)\, d\theta = \text{prob}\{\theta \leq \Gamma(\mathbf{x}, t) < \theta + d\theta\} \tag{3}$$

to monitor the reduction of concentration values. This function has central moments

$$\begin{aligned} m_n(\mathbf{x}, t) &= \int_0^\infty (\theta - \overline{\Gamma(\mathbf{x}, t)})^n\, p(\theta; \mathbf{x}, t)\, d\theta & (4) \\ &= \overline{\left(\Gamma(\mathbf{x}, t) - \overline{\Gamma(\mathbf{x}, t)}\right)^n}, & (5) \end{aligned}$$

with the mean, $\overline{\Gamma(\mathbf{x}, t)}$ defined by

$$\overline{\Gamma(\mathbf{x}, t)} = \int_0^\infty \theta\, p(\theta; \mathbf{x}, t)\, d\theta. \tag{6}$$

The second central moment $m_2(\mathbf{x}, t)$ often serves as a measure of the magnitude of fluctuations.

Experiments show a distinction between the mean and the higher ordered moments. The mean $\overline{\Gamma}$ has little sensitivity to either space or time averaging or to molecular diffusivity [CS90b]. A good approximation to the ensemble average value requires fewer realizations than the higher moments. A large body of work examines the properties of the mean concentration and shows considerable progress towards predicting $\overline{\Gamma}(\mathbf{x}, t)$ [MY71, pages 606–676], [SY91]. The mass conservation equation, which is linear in $\overline{\Gamma}$, allows use of the superposition principle and point sources.

However the mean tells you nothing about concentration reduction, as it can come from instantaneous values consistently close to the mean value, or from instantaneous values which fluctuate between lower concentrations and much higher intermittent concentrations.

Moments higher than the mean show sensitivity to both temporal and spatial averaging and to molecular diffusivity. Only molecular diffusivity can reduce the moments of the concentration distribution integrated over the entire cloud [CS90a]. Further [CS79] showed that one could not consider higher moments generated from an ideal point source, unlike the case for $\overline{\Gamma}$. Fackrell and Robins [FR82] confirmed this experimentally. The complexities of an environmental flow lead one to ask, "What can experiments actually measure?" [Sul90]. Recall the "necessity for validation" raised earlier. This leads to the development of *Cloud Average Statistics* [SY93] as a concept. Alas, researchers have not yet designed experiments to fully explore this approach.

This thesis will introduce a statistical measure that contains relevant information on the dilution process and places a premium on rapid convergence, *i.e.* reduces the epoch required for repeated trials in a slowly varying process.

1.3 Instrument Smoothing

The texture of the contaminant cloud, with very thin sheets and strands, leads to a spatial and temporal experimental resolution problem. This thesis defines $\Gamma(\mathbf{x}, t)$ as a "perfect" measurement, *i.e.* one with continuum scale temporal and spatial resolution. It does not depend on instrumentation. Considering time and space averaged values of $\Gamma(\mathbf{x}, t)$ changes the basic governing equations [Sul84]. Researchers have attempted to separate the averaging process from the instantaneous values of concentration by the use of an intermittency factor. However this leads to considerable

difficulties in the definition of a "threshold" value below which analysis considers Γ to be zero. This depends on instrumentation in its conventional application [CS89]. Measured values generally have a threshold criterion where instrument noise has the same magnitude as signal level and analysis has difficulty distinguishing the two [LC94]. Contaminant concentration measurements require care to interpret. For a review, see [MCS93].

In toxicological applications other processes, *e.g.* breathing or air conditioning filters, may smooth out the strand-sheet structure. This thesis will work with a well-defined, instrument independent measure. Fluid can pass through any device and the effect of the device can be monitored by using the same measure on the exit side. A discussion of the theoretical advantages of the proposed new measure in Section 2.4 will say more about instrument effects.

1.4 A New Measure of Contaminant Concentration Reduction

This section introduces a measure which has a clear and immediate interpretation with relevant information content and which converges with few realizations. Earlier papers [CS90a] and [SY93] introduced the concept of *cloud-averaged* statistics. They illustrated the intuitive advantage of using concentration values throughout the entire cloud in each realization to promote rapid convergence of statistics. Measurements to explore that theory do not yet exist. This thesis seeks a similar advantage for the more conventional measurements made as a cloud passes a fixed point, say $\mathbf{x}_0$, in space. Few suitable measurements on the important problem of a diffusing contaminant cloud exist, with the notable exception of the experiment conducted at the Warren Spring Laboratory by D.Hall *et al* [HWM+91] which this thesis will analyze in the

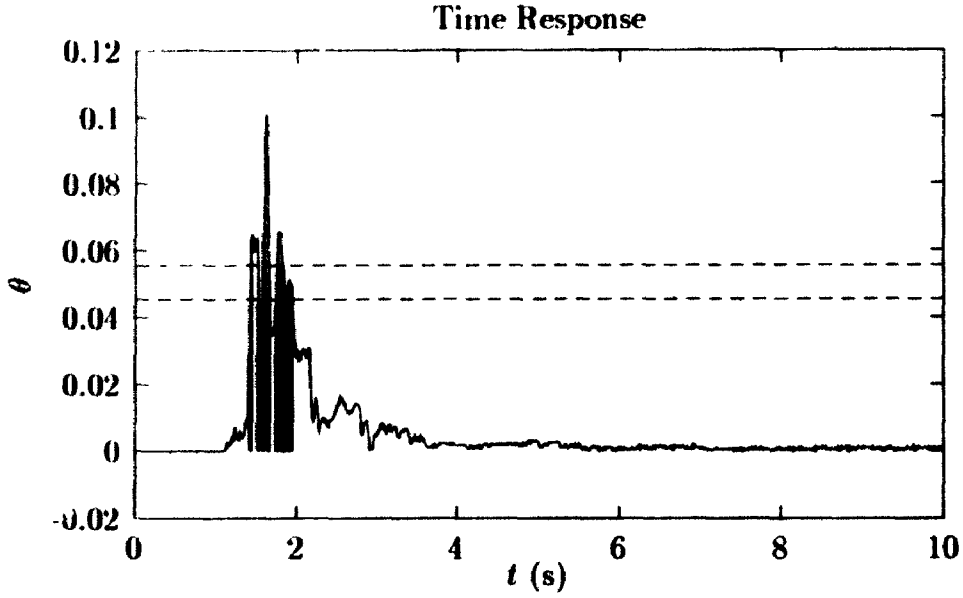

Figure 1: Fraction of dose from times when concentration falls within a specified range of concentration

new framework set out here.

An aspirating probe withdraws fluid with concentration values $\Gamma(\mathbf{x}_0, t)$ at a constant speed u through a probe of area δA for a sample time δt. The i'th sample has volume $u\,\delta A\,\delta t$ and contains a mass of contaminant Q_i to give a concentration of $\theta_i = Q_i/u\,\delta A\,\delta t$. If n samples have concentration such that $\theta \leq \theta_i < \theta + \delta\theta$ then the total mass in that interval,

$$\sum_{\theta \leq \theta_i < \theta + \delta\theta} Q_i \tag{7}$$

can be used to represent the fraction of the total mass sampled that is found in the selected interval. In Figure 1, the shaded area corresponds to that part of the dose coming at concentrations within the interval marked by the dashed lines. The corresponding contribution to the mass fraction is shown in Figure 2. The expected value of this measure, normalized by the bin width $\delta\theta$ and by the expected value of the dose as defined in equation (9), then gives the expected mass fraction. This

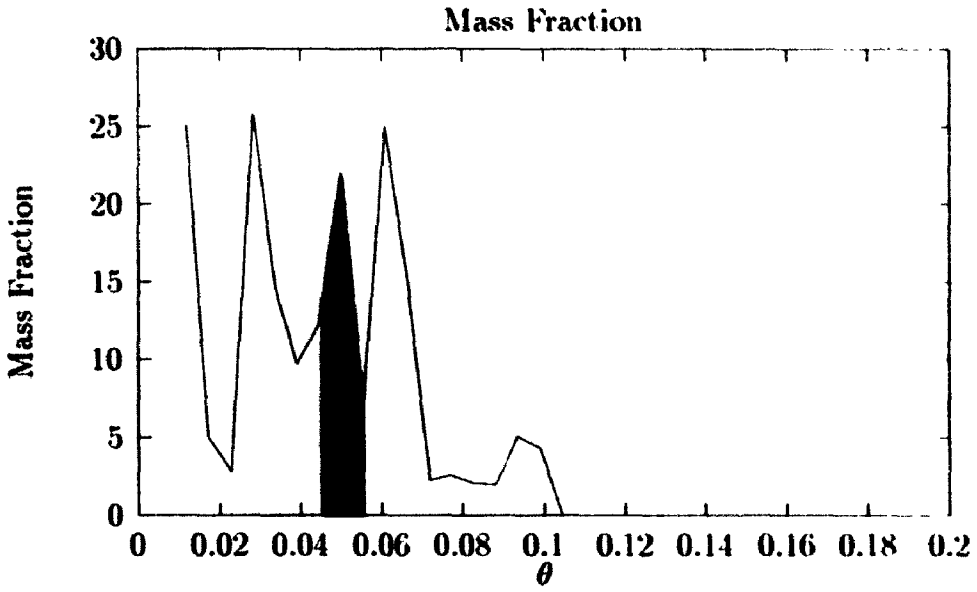

Figure 2: Contribution to mass fraction of area shaded in Figure 1.

compares with the conventional random variable, dosage,

$$d(\mathbf{x}_0) = \int_{-\infty}^{\infty} \Gamma(\mathbf{x}_0, t)\, dt, \tag{8}$$

and its expected value,

$$\overline{d(\mathbf{x}_0)} = \int_{-\infty}^{\infty} \overline{\Gamma(\mathbf{x}_0, t)}\, dt, \tag{9}$$

which has the interpretation that $\overline{d(\mathbf{x}_0)}\, u\, \delta A$ gives the expected total mass aspirated as a cloud passes the fixed sampling station at $\mathbf{x}_0$. Section 4.2 will discuss the variability of the mass fraction, in a given concentration interval, from realization to realization. It has variability comparable with that of $d(\mathbf{x}_0)$. The expected mass fraction monitors the concentration dilution process and also permits an assessment of the amount of mass (or exposure time) occurring, for instance, above a critical threshold level of concentration in a toxicological context. Significant theoretical advantages in using the expected mass fraction follow from its derivation, in the following section, from the one-point probability density function. Section 2.4 shows how, using the α-β prescription of Chatwin and Sullivan [CS90b], the lower ordered moments

of the probability density function relate simply to those of the expected mass fraction. Through inversion, the moments can provide a predictive capability for a good approximation to the expected mass fraction.

Chapter 2

Expected Mass Fraction

2.1 Introduction

This chapter defines the new measure, the *expected mass fraction* (EMF). Should a storage vessel rupture and release a cloud of toxic gas into the atmosphere, emergency personnel need to model the flow and predict the evolution of the contaminant concentration field. One conventional measurement used to assess toxicological impact is the random variable dosage, $d(\mathbf{x})$, as defined in equation (8), with the ensemble average value $\overline{d(\mathbf{x})}$. Dosage measures the total concentration exposure as the contaminant cloud passes at a fixed position in space $\mathbf{x}$. The new measure, the EMF, describes the distribution of dosage over different concentrations. It depends only on the one-point probability density function $p(\theta; \mathbf{x}; t)$. Further, using results shown in [CS90b] and extensions thereto, simple expressions for the lower-ordered moments of the probability density can provide estimates for the probability density function and hence for the EMF. The estimates of the EMF have a variability, from realization to realization, comparable with that of estimates of the dosage, as defined by equation (8).

Since equation (8) involves an integral over time, as the cloud evolves relatively

few realizations will adequately approximate ensemble average statistics on $d(\mathbf{x})$. Limitations exist in both the theoretical prediction of dosage and in the correlation of dosage with toxicological impact. $d(\mathbf{x})$ is determined by a probability density function which depends jointly on many points in time. Furthermore toxicological impact in many cases will depend only on the amount of contaminant at concentration values above a prescribed threshold value.

2.2 Theoretical Foundation

Consider a contaminant cloud as it passes the fixed position located by the vector $\mathbf{x}_0$. Equations (3) and (4) define the one-point probability density function $p(\theta; \mathbf{x}, t)$ and its moments. This fundamental measure can track the reduction of concentration values within the evolving contaminant cloud. Define an expected time of residence for concentration at the fixed position $\mathbf{x}_0$ as

$$p'(\theta; \mathbf{x}_0) = \int_{-\infty}^{\infty} p(\theta; \mathbf{x}_0, t) dt \tag{10}$$

so that $p'(\theta; \mathbf{x}_0) d\theta$ represents the average time per release during which the concentration is between θ and $\theta + d\theta$. The corresponding total moments are

$$\begin{aligned} M_n'(\mathbf{x}_0) &= \int_{-\infty}^{\infty} M_n(\mathbf{x}_0, t) dt & (11)\\ &= \int_{-\infty}^{\infty} \int_{0}^{\infty} \theta^n p(\theta; \mathbf{x}_0, t) d\theta \, dt & (12)\\ &= \int_{0}^{\infty} \theta^n \int_{-\infty}^{\infty} p(\theta; \mathbf{x}_0, t) \, dt \, d\theta & (13)\\ &= \int_{0}^{\infty} \theta^n p'(\theta; \mathbf{x}_0) \, d\theta. & (14) \end{aligned}$$

where

$$M_n(\mathbf{x}, t) = \int_{0}^{\infty} \theta^n p(\theta; \mathbf{x}, t) \, d\theta \tag{15}$$

and

$$M_1'(\mathbf{x}_0) = \int_{-\infty}^{\infty} \overline{\Gamma(\mathbf{x}_0, t)} dt = \overline{d(\mathbf{x}_0)}, \tag{16}$$

from (11) and (9). Now define the new measure, the EMF, as

$$\hat{p}(\theta; \mathbf{x}_0) = \frac{\theta p'(\theta; \mathbf{x}_0)}{M_1'(\mathbf{x}_0)}. \tag{17}$$

The moments of $\hat{p}(\theta; \mathbf{x}_0)$ are related simply to those of $p'(\theta; \mathbf{x}_0)$:

$$\begin{aligned} \hat{M}_n(\mathbf{x}_0) &= \int_0^\infty \theta^n \hat{p}(\theta; \mathbf{x}_0) d\theta & (18) \\ &= \int_0^\infty \theta^{n+1} p'(\theta; \mathbf{x}_0) d\theta / M_1'(\mathbf{x}_0) & (19) \\ &= M_{n+1}'(\mathbf{x}_0)/M_1'(\mathbf{x}_0) & (20) \end{aligned}$$

so that,

$$\hat{M}_0(\mathbf{x}_0) = \int_0^\infty \hat{p}(\theta; \mathbf{x}_0) d\theta = 1. \tag{21}$$

The interpretation of (17) is that $\hat{p}(\theta; \mathbf{x}_0)\, d\theta$ is the expected fraction of the "total mass" $\overline{d(\mathbf{x}_0)}$ (within the continuum scale volume element surrounding $\mathbf{x}_0$) in the concentration interval ($\theta \leq \Gamma(\mathbf{x}_0, t) < \theta + d\theta$). The value of θ for which $\hat{p}(\theta; \mathbf{x}_0) = 0.5$, for example, is the concentration for which, on average, one half of the total mass passing $\mathbf{x}_0$ has higher concentrations. The EMF defined in (17) has the advantage over dosage $\overline{d(\mathbf{x}_0)}$ as defined in (9) that it clearly designates the manner in which contaminant mass is distributed over concentration values. Equation (17) is particularly convenient in circumstances where there is a non-linear biological response to concentration values, and we anticipate improved correlations between stimulus and response to concentration values using the EMF in toxicological impact studies.

In what follows a case will be made for the advantages of (17) in the difficult problem of extracting useful information from both field and laboratory experiments, and also for the advantages of (17) in the context of furthering the development of a theoretical predictive capability.

2.3 Experimental Advantages

As mentioned in Section 1.2, estimating ensemble average values requires a repeated release in a large number of trials. Because environmental flows and to some extent laboratory flows (especially when electronics are included) slowly change one wants to keep the time interval required to perform these trials as small as possible.

It is anticipated (and verified when discussing measurements later) that the EMF, which is defined by a time integral, will have a variability that is comparable with dosage and will provide information which is more relevant. By comparison, it would require a relatively large number of repeated releases to measure representative values of the distributed measure $m_n(\mathbf{x}_0, t)$ defined in equation (4) even for $n \leq 4$ and an unrealistically large number of repetitions to approximate the probability density $p(\theta; \mathbf{x}_0, t)$.

In general it is expected that a very good representation of a probability density function can be achieved by inverting the lowest four moments using for example a maximum entropy formalism [DSY94, DS90]. One can simply measure the moments of the concentration

$$M'_{n+1}(\mathbf{x}_0) = \overline{\int_{-\infty}^{\infty} \Gamma^{n+1}(\mathbf{x}_0, t)\, dt} \tag{22}$$

for, say, $n \leq 5$ and determine the total moments $\hat{M}_n(\mathbf{x}_0)$ from (18) and hence by inversion estimate the EMF, $\hat{p}(\theta; \mathbf{x}_0)$, as defined in (17).

Equation (22) is a very simple measurement that could in principle be recorded on-line using analogue devices. One could also compile $\hat{p}$ directly from experimental records as

$$\hat{p}(\theta; \mathbf{x}_0) = \frac{d}{d\theta} \int_{-\infty}^{\infty} \overline{H(\Gamma(\mathbf{x}_0, t) - \theta)}\, dt / M'_1(\mathbf{x}_0), \tag{23}$$

where $H(\theta)$ is the Heaviside unit step function.

Note also that, because $\Gamma(\mathbf{x}_0, t)$ and hence $\hat{p}(\theta; \mathbf{x}_0)$ are defined on a continuum

scale, other values averaged over an arbitrary sample area, say $A(\mathbf{x}_0)$, are simply

$$\hat{p}_A(\theta;\mathbf{x}_0) = \int_{A(\mathbf{x}_0)} \theta\, p'(\theta;\mathbf{x})\, dA(\mathbf{x}) / \int_{A(\mathbf{x}_0)} M_1'(\mathbf{x})\, dA(\mathbf{x}) \tag{24}$$

A probe making measurements with this same sample area will not give the same result as an ideal probe measuring at the continuum level, as discussed in Section 1.3.

This measure, more simple than $p(\theta;\mathbf{x}_0,t)$, represents a means of monitoring the way a contaminant cloud is diluted by monitoring the shift of area under $\hat{p}$ to smaller values of θ. It should provide useful information for the purpose of toxicological impact. Because the measure does not have physical assumptions built into it, it places no restrictions on chemical reactions, density effects, etc. The variability of $\hat{p}(\theta,\mathbf{x}_0)$ will be discussed using the Warren Spring data in Section 4.2.

2.4 Theoretical Advantages

Whereas the dosage of equation (8) depends on a joint probability density function of many points in time, the definition of expected mass fraction in equation (17) depends only on a one-point probability density function. Chatwin and Sullivan [CS90b] have provided a simple form for the central moments of the contaminant field. The derivation is outlined in Appendix A. Their expression for the distributed moments, applied to a contaminant cloud and written in extended form, is

$$m_n'(\mathbf{x}_0,t) = \beta^n(t) C_0^n(t) \left(\chi(\alpha(t)-\chi)^n + (-1)^n(\alpha(t)-\chi)\chi^n\right)/\alpha(t), \tag{25}$$

where $C_0(t)$ is the largest value of $\overline{\Gamma(\mathbf{x}_0,t)}$ in the cloud at time t and $\chi(\mathbf{x}_0,t) = m_1(\mathbf{x}_0,t)/C_0(t)$. The functions $\alpha(t)$ and $\beta(t)$ pertain to the entire cloud at time t. Equation (25) has received experimental verification for lower order moments in a variety of flows with continuous release, most notably in [SS94]. We will show, in discussing experiments, indirect evidence suggesting the applicability to clouds. In

equation (25) the moments are expressed in terms of $\overline{\Gamma(\mathbf{x}_0, t)}$, which is relatively insensitive to instrument smoothing and presumed to be the most rapidly converging measure available. Considerable progress has been made towards its prediction [SY91].

The basic idea from a predictive viewpoint is to generate $\alpha(t)$ and $\beta(t)$ and hence the lower ordered moments from equation (25). The central moments from equation (25) are converted to (absolute) moments $M_n(\mathbf{x}_0, t)$ and, through equations (11) and (18), used to generate $\hat{M}_n(\mathbf{x}_0)$ which in turn are used through inversion to generate the expected mass fraction $\hat{p}(\theta; \mathbf{x}_0)$ given in equation (17).

Chatwin and Sullivan [CS90a] provide an exact expression for the spatially integrated moments:

$$\frac{d}{dt}\int_{a.s.} \overline{\Gamma^{n+1}}\, dv = -n(n+1)\kappa \int_{a.s} \overline{\Gamma^{n-1}(\nabla\Gamma)^2}\, dv, \tag{26}$$

where "$a.s.$" denotes an integral over all space. Moseley [Mos91], in some preliminary numerical work accomplished closure for this expression by using

$$\nabla\Gamma \propto \frac{\Gamma(\mathbf{x}, t) - \theta_t}{\lambda}, \tag{27}$$

where θ_t is a background threshold value of concentration and λ is the conduction cut-off length (defined in equation (2)), along with equation (25). Labropulu and Sullivan [LS94] have been able to derive analytic expressions for $\alpha(t)$ and $\beta(t)$ that are in reasonable agreement with experimental measurements. This procedure has the advantage that closure is effected on physical grounds and on a term that appears under an integral over all space.

Return now to the problem of spatial and temporal experimental resolution in the context of the α-β prescription of moments. This problem was addressed in [CS87] which concluded that α would be relatively unaffected by improved resolution while β in contrast would significantly increase with improved spatial and temporal resolution.

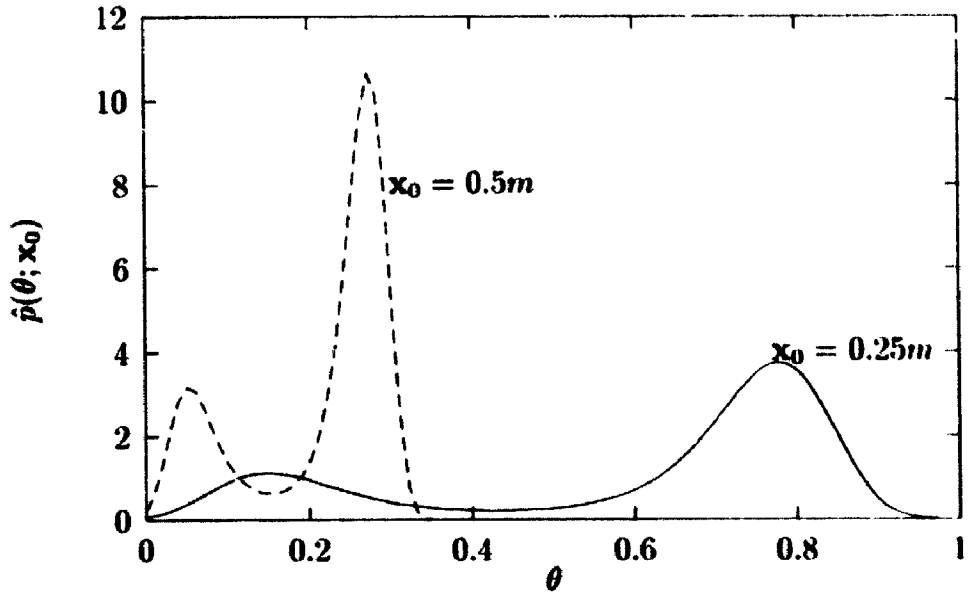

Figure 3: Change in the expected mass fraction function with distance downstream

Measurements by Sakai *et al* discussed in [CS93] using four different probes ranging in sample volume from $(0.54\text{mm})^3$ to $(0.10\text{mm})^3$ confirmed the α-β description for each probe size and showed α to be effectively unchanged with ~4% maximum irregular departure from a mean value of 1.30, while the value of β^2 doubled from 0.16 to 0.33 in going from the probe with the largest sample volume to the probe with the smallest volume. It would seem worthwhile to develop an extrapolation procedure (*c.f.* [DS87]) to estimate the continuum values of β^2, in particular for field experiments. Note in this context the "plateau effect" shown in the heuristic developed by Carn and Chatwin [CC85]. There it was shown that, if the measurement scale was sufficiently coarse, measurements with half that scale would not produce significant change. That is, one needs to have spatial resolution comparable with the conduction cut-off length λ to see appreciable change with improved resolution.

This analysis gives the expected mass fraction, not the variability or the probability distribution. We later estimate the variance of the statistic, the EMF.

2.5 Example

A cloud of tracer is released instantaneously in grid turbulence, and the time-varying concentration is measured downstream at two points. For typical parameters use values from [War84]. The cloud has an average concentration distribution which we assume to be Gaussian, such that

$$\overline{\Gamma}(\mathbf{x},t) = \frac{Q}{(\sqrt{2\pi}\sigma(t)^2)^{3/2}} \exp\left(-\frac{(x-ut)^2+y^2+z^2}{2\sigma(t)^2}\right). \tag{28}$$

where

$$\sigma(t) = \sqrt{Dt}, \tag{29}$$

$$u = 7\text{m/s}, \tag{30}$$

$$D = 0.0004\text{m}^2/\text{s}. \tag{31}$$

Q, the total amount of tracer, will be normalized to give unit dosage at the upstream sampling point. The concentration is measured downstream of the release point at distances of 0.25m and 0.5m. Because the cloud moves past the sample point with time, the trailing edge has slightly more time to develop than the leading edge, so the mean concentration as a function of time is not exactly symmetric about the mode of the concentration function. Assuming typical values of $\alpha = 1.5$ and $\beta = 0.5$ a maximum entropy method can be used [DS90, Appendix C] to calculate the EMF using four moments as calculated by equation (18). The results are shown in Figure 3. Notice the shift to lower concentrations at the downstream point.

To repeat, there is a good prospect of predicting the EMF, in contrast to dosage or exceedance statistics.

Chapter 3

Warren Spring Laboratory Measurements

As mentioned in Chapter 1 there are lamentably few adequate laboratory measurements of a diffusing cloud and no suitable field measurements. One notable exception is the data made available to us by Dr. David Hall of the Warren Spring Laboratory in Great Britain. These are remarkable in that they have up to 100 repeated trials for the release of identical gas clouds. We are indeed grateful to have this data set.

3.1 Description of Experiments

Warren Spring Laboratory performed a very useful series of wind tunnel tests modelling the instantaneous release of a cloud of gas. The experiments were designed to investigate the dispersion of a heavy gas for Richardson numbers between zero and 10. The importance of this data comes from the 50 or 100 repetitions of the gas release for each case, giving sufficient data to calculate ensemble averages and other useful statistics on a non-stationary experiment. The bulk Richardson number for

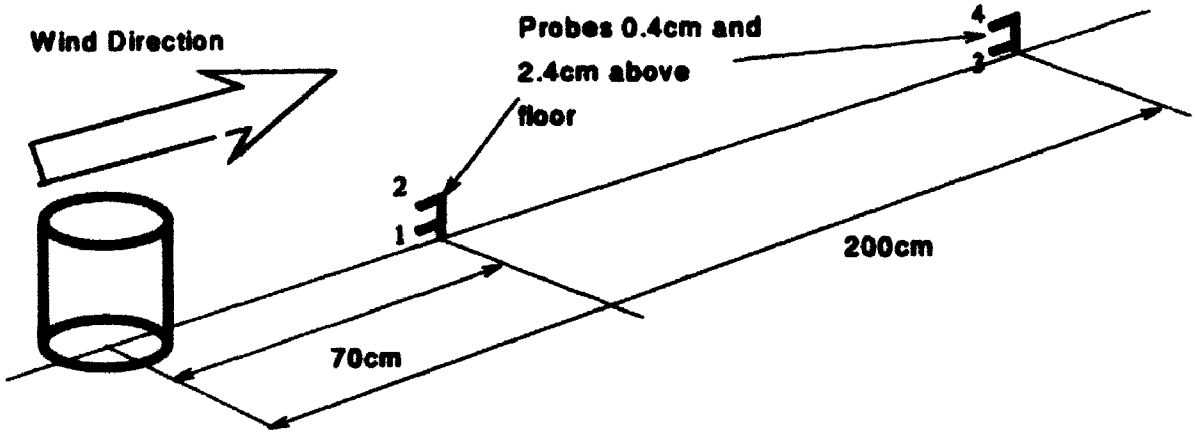

Figure 4: Schematic drawing of experimental setup. After [HWM+91].

these experiments was defined as

$$R_i = g\frac{(\rho_{gas} - \rho_{air})}{\rho_{air}}\frac{L}{U^2}, \tag{32}$$

where g is gravitational acceleration, ρ_{gas} and ρ_{air} are the densities of the tracer gas and the ambient air respectively, L is a characteristic length scale, taken as 13cm, the height of the tent, and U is the mean incident windspeed at a height of 13cm.

The experiments, documented in [HWM+91], modelled the instantaneous release of a cylindrical volume of (heavy) gas at a solid surface into the boundary-layer flow. Figure 4 sketches the experimental setup. The gas was released by collapsing an enclosing cylinder, so that initially the tracer was stationary relative to the incident flow. Tracer concentrations were measured at two heights at each of two measuring positions downstream, on the centerline of the flow past the release point.

The cylinder containing the gas was 13cm high and 14cm in diameter, with a fixed roof to ensure that no gas escaped before the release. The sampling probes were located downstream on the centerline at a distance of 70cm and 200cm, and at a height of 0.4cm and 2.4 cm. They were of the aspirating variety. The released gas consisted of either Bromo Chloro di-Fluoro methane (chemical formula $CBrClF_2$) (BCF), or of argon with methane as the tracer. In the first case, catharometers measured

Test Number	Bulk Richardson number	u_{ref} m/s	No. of Realizations
1	0	0.98	100
2	0.5	0.98	100
3	1	1.74	100
4	2	1.2	100
5	5	1.1	50
6	10	0.78	50

Table 1: Test Parameters

Probe Number	Distance Downstream (cm)	Height above Surface (cm)
1	70	0.4
2	70	2.4
3	240	0.4
4	240	2.4

Table 2: Probe Positions

concentration of BCF, while flame ionization detectors measured the argon/methane mixture concentration. The release, or collapse, time of the tent was estimated at about 0.2 seconds. The area over which the probes measured, based on the aspiration rate of the probes and the typical wind speeds, had a radius on the order of 1mm. The samples were measured at a rate of 100Hz, giving a sample "length" of about 0.5 - 1cm based on the reference wind speed.

The boundary layer in the wind tunnel was developed by initial fences and wedges, followed by appropriate roughness elements on the floor of the tunnel to develop the desired wind speed profile. The profile approximates a constant-stress logarithmic layer at the test site, with z_0 of 0.05 - 0.1mm, modelling atmospheric flow over a surface of moderate roughness. Since the release cylinder dimensions were 1:100 full scale, this represents a full scale z_0 of about 5-10 cm full scale, representative of open grassy terrain. Reference wind speeds were measured at the height of the top of the model, 13cm. Some of the relevant details are included in Tables 1 and 2 . Figure 5 shows a partial set of time histories, in this case for Probe 1 and Richardson number

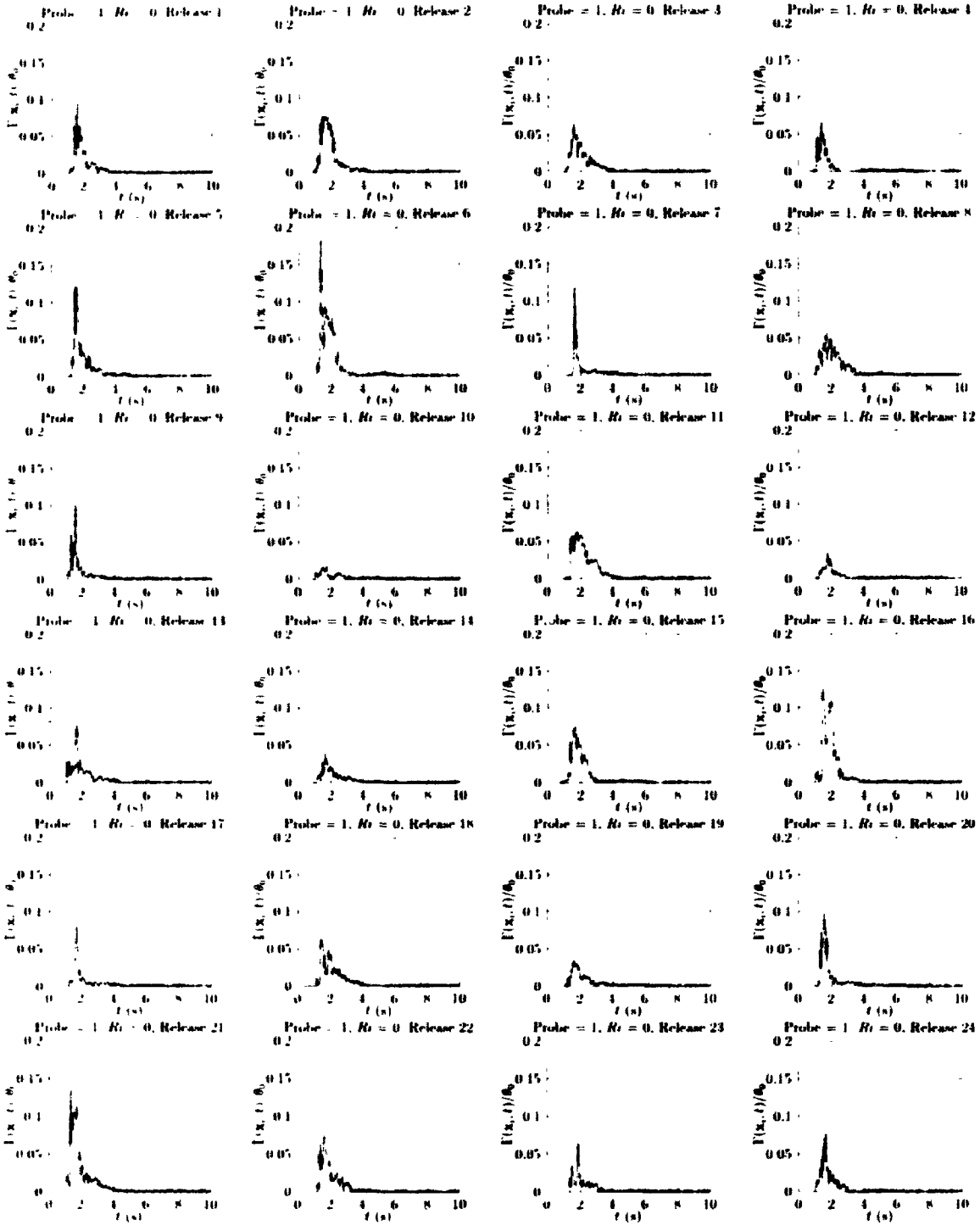

Figure 5: Typical records of individual releases from Test 1, Probe 1.

0, and Figure 6 shows the average concentration for all tests as a function of time from release. One data set, for test 6, probe 4, was damaged in transmission and has not been replaced. Thus results are shown for only 23 cases.

The data analysis has involved several approaches. The primary one for this thesis involves looking at the EMF and its variability. A secondary aspect has been the time dependence of the EMF, and the possibility of normalizing the time histories by the change in reference concentration (C_0) to verify that the cloud evolves in the expected fashion [Bat64].

The initial distribution of contaminant does not resemble a point source. It has dimensions about 1/5 the distance downstream to the closer probe position, and an initial height, 13cm, much greater than the probe height of 0.4cm or 2.4cm. Nonetheless, assuming an elevated point source as suggested by [Bat64] produces a reasonable approximation to the observed behavior.

The following sections and Chapter 4 examine the data in detail. Appendix B provides additional information about the Warren Spring data and the analysis. In summary, the data behaved in a reasonable fashion, and fitted a theoretical model better than expected, considering the differences between the experimental and theoretical models.

3.2 Dosage

The integral of concentration over time, at a particular point $\mathbf{x}$, defines the dosage:

$$d(\mathbf{x}) = \int_0^\infty \Gamma(\mathbf{x}; t)dt \tag{33}$$

The experimental equivalent of this is simply the sum of the concentration readings for a particular run, times the time increment, 0.01s:

$$d'_k(\mathbf{x}) = 0.01 \times \sum_{i=0}^{N} \theta'_{k,i} \tag{34}$$

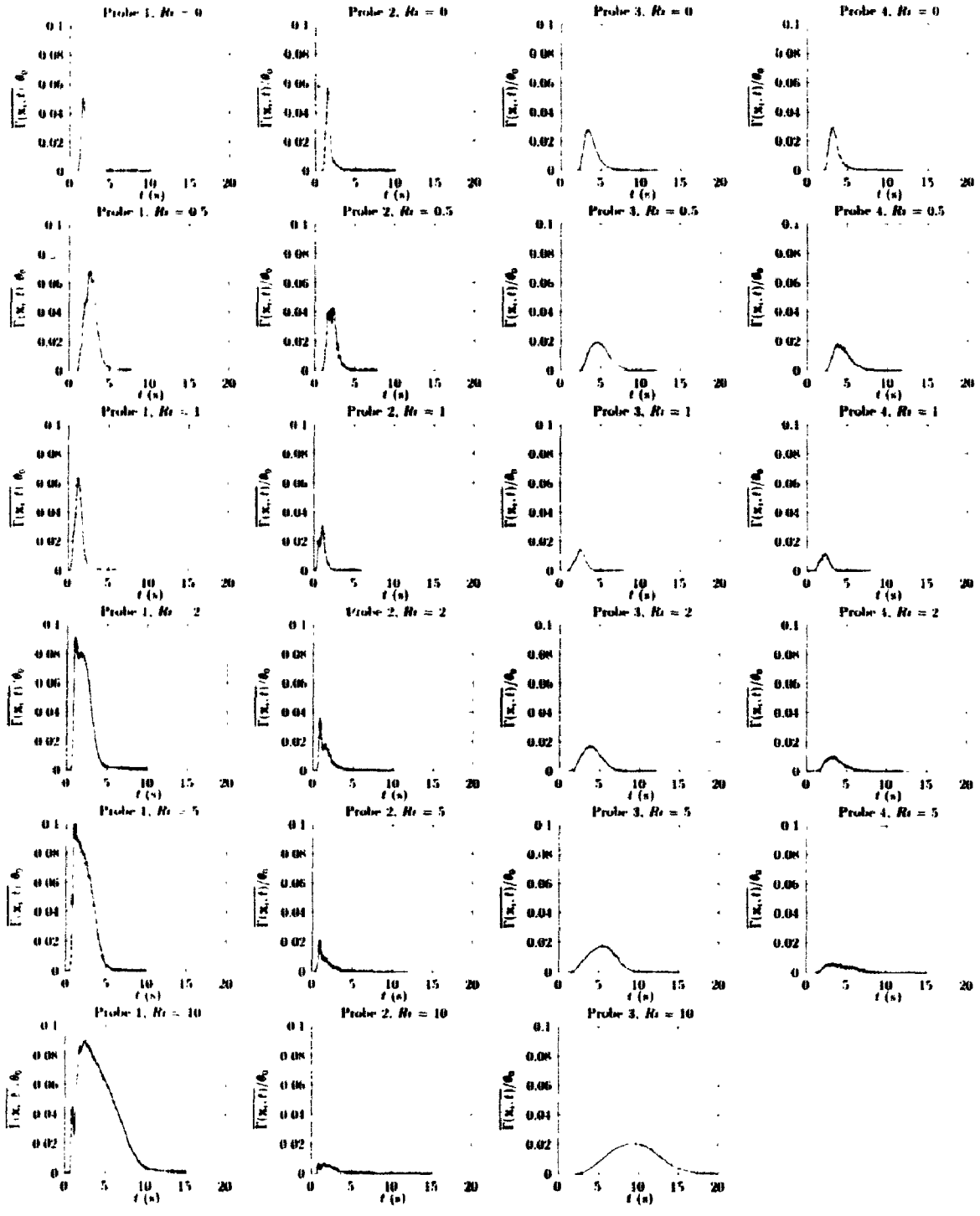

Figure 6: Average response with time.

where $\theta'_{k,i}$ is the i'th observed concentration reading out of N for the k'th run of the particular experiment. Appendix B discusses an experimental drift problem which this measure revealed. Figure 7 shows the convergence of estimates of the expected dosage with increasing number of realizations, incorporated in the order in which the results were obtained, after drift correction.

3.3 Probability of concentration

The second step of the data analysis was to examine the probability distribution of concentration as a function of time. In particular we looked at the relationship between the mean and the variance at each time step. This indicated a strong relationship, although not necessarily what was expected. The plot of mean *vs* variance tended to look like a loop, especially on a log-log plot. The slope changed from about 1 to about 2 with time. Before the peak concentration, the slope was about 1 and after the peak about 2, with a transition section between. This agreed with the dimensional idea of variability scaling with both the mean and the initial concentration, as in the case of the α-β model [CS90b], and later, as the initial concentration was lost, scaling only on the mean, the only available reference concentration. Figure 8 shows this relationship. The arrows indicate the direction of change with time. The arrow pointing to the right marks the earlier part of the record and has a slope of 1. The arrow pointing to the left marks the later part of the record and has a slope of 2.

3.4 EMF

Next the Expected Mass Fraction was calculated. Two approaches were possible. The first was simply to divide the concentration range up into bins, and count the number

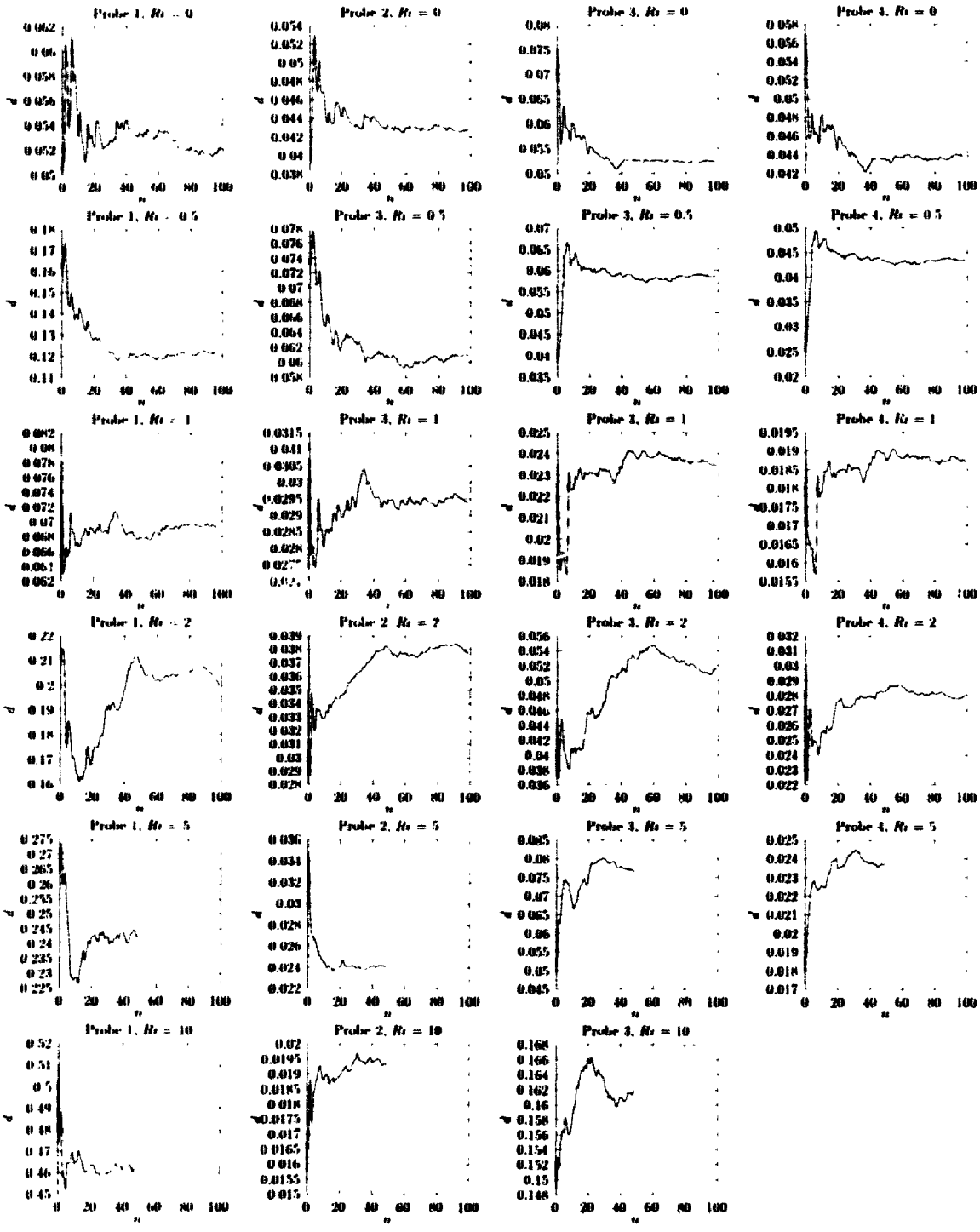

Figure 7: Cumulative average of dosage (Individually scaled). The plots refer to probes 1–4 going from left to right, and to tests 1–6 going from top to bottom.

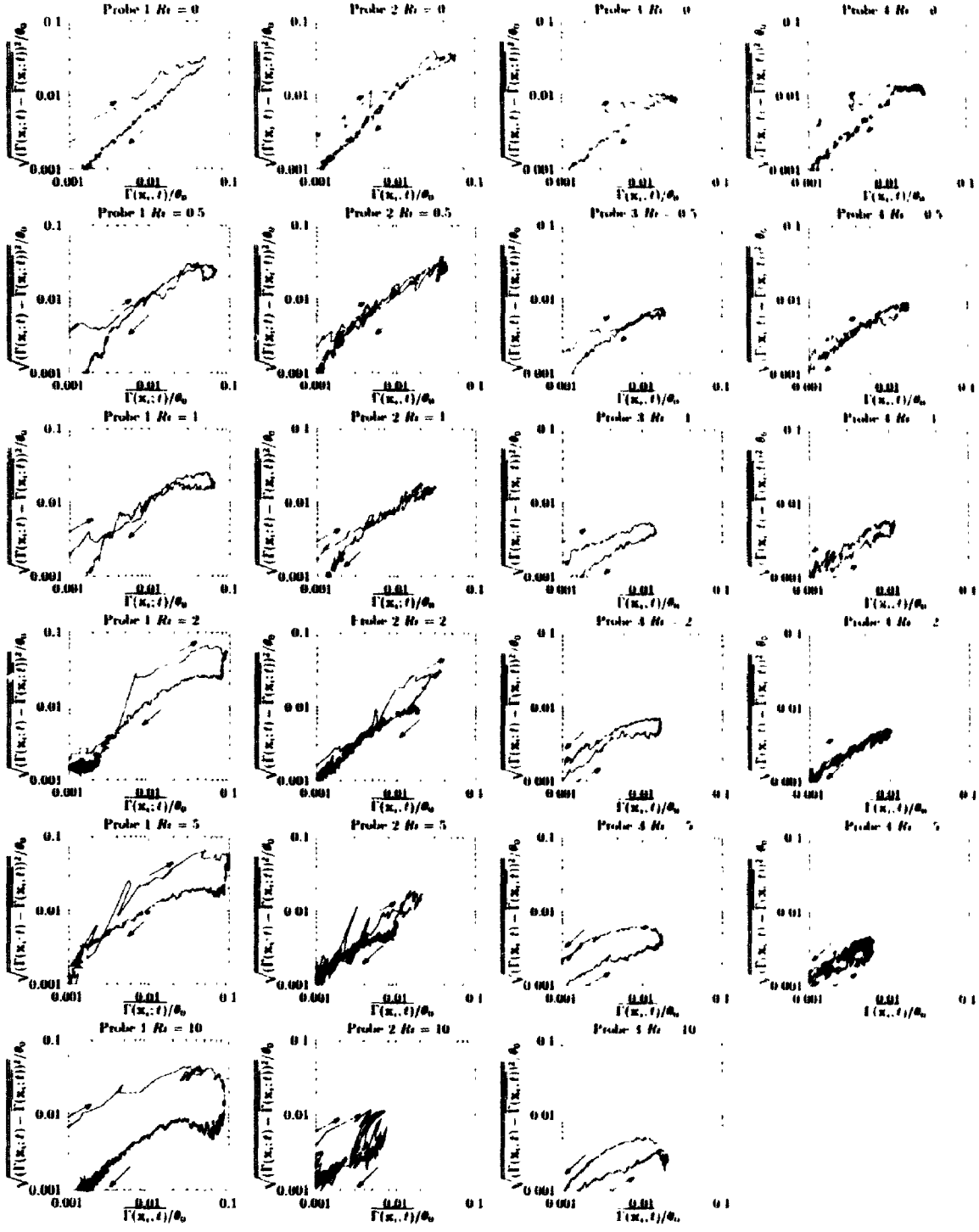

Figure 8: Standard Deviation of Concentration *vs* Average Concentration. The arrows indicate change with time. The arrow pointing towards the right, indicating the early part of the record, has a slope of 1. The other arrow, indicating later time, has a slope of 2.

of occurrences in each bin. The second was to sort the data, calculate the running sum and interpolate at a fixed number of points, to get the dosage within each range. This approach was the one used. Over most of the range, the two approaches give the same result. However, at the lowest concentrations, there may be many points at the zero concentration end of the bin, skewing the center of mass of the distribution within the bin. In this case, the second method appears preferable, as it reflects the actual "mass" in each bin. Figure 9 shows the EMF plotted with the dots showing the result for 8 bins, and the line the result for 64 bins.

As the dosage is formed from the sum of the individual mass fractions, its intensity (standard deviation divided by mean) is less than that of individual bins of the EMF. Figure 10 shows the intensity of the EMF estimate divided by the intensity of the corresponding dosage. Most of the variability of the dosage comes from the few high-concentration data points, and they reflect this with intensities typically 10 times the intensity of the dosage.

3.5 Conclusion

This data provides reasonably shaped curves for the EMF. The EMF clearly shows the reduction in concentration with probe position, and also the reduction in dosage downstream. While the peak value remains almost constant, the peak becomes much narrower. Although comparable with the variability of dosage, the variability of estimates of the EMF is large and warrants further exploration in Chapter 4.

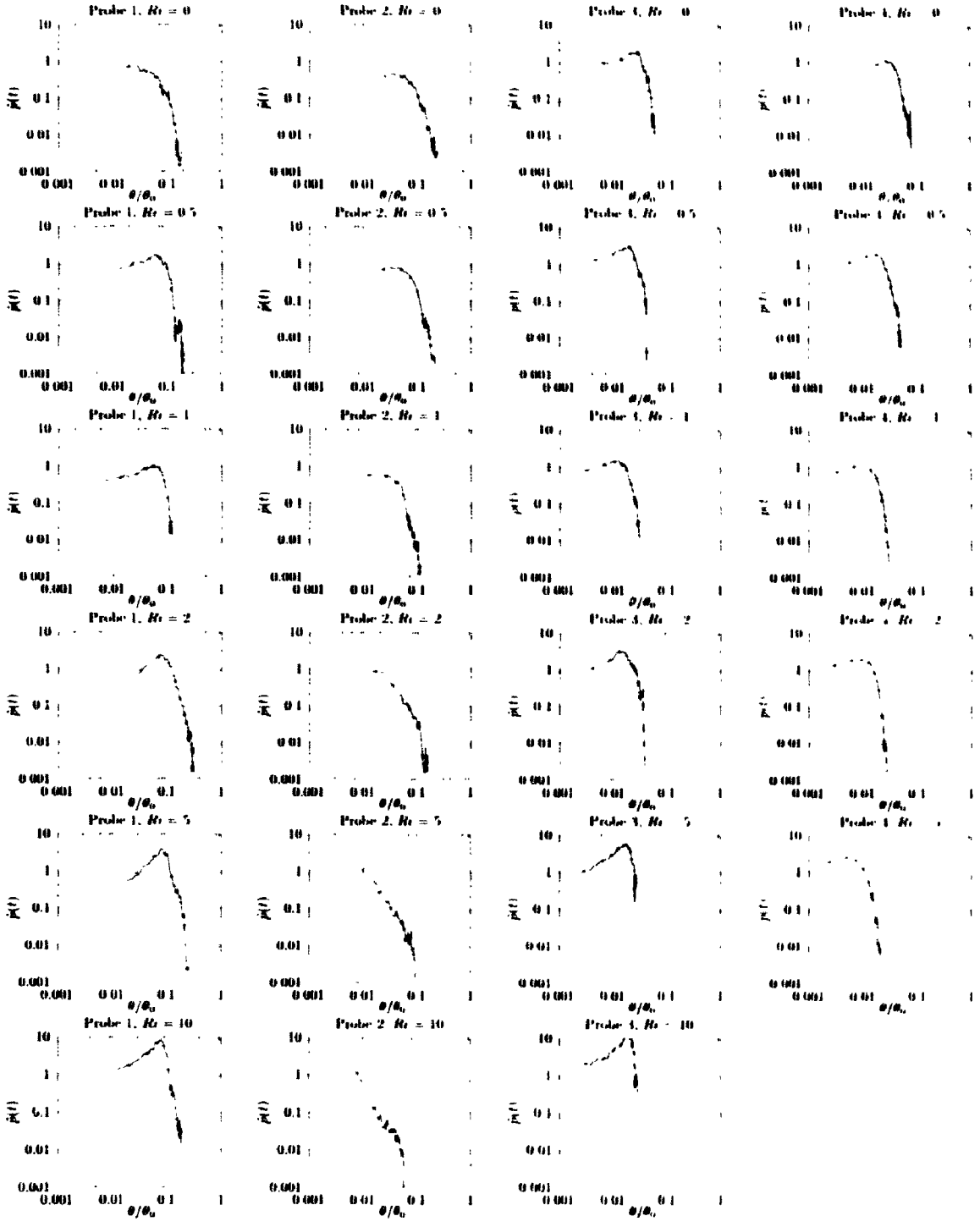

Figure 9: EMF calculated with 8 bins (points) and with 64 bins (line).

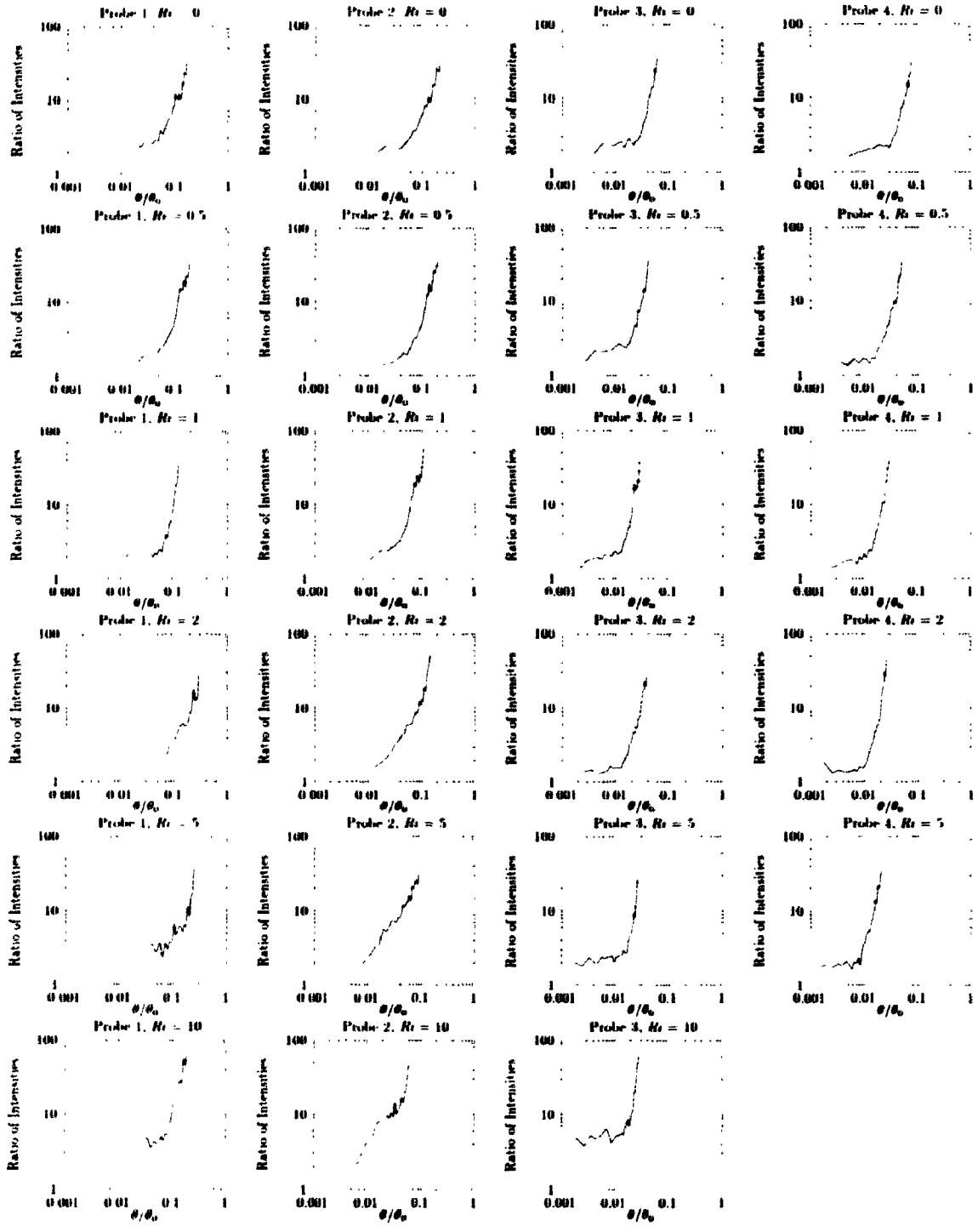

Figure 10: Intensity of EMF divided by intensity of dosage.

Chapter 4

Variability and Trend

The question to be investigated is how far in individual clouds the expected mass value (or exposure) in a given concentration interval departs from the average. This information is significant for instance in attempting to assess the likely consequence of a sudden release of toxic or inflammable contaminant.

4.1 Physical Reasons for Variability

Consider the hypothetical case of $\kappa = 0$. If the cloud in its entirety is considered [SY93], then for conserved release quantity Q, all of Q at all time would be found in release concentration θ_0 and the EMF would be a δ-function at θ_0. If $\kappa \neq 0$ is considered then the expected mass fraction would have non-zero values for $\theta < \theta_0$, for $t > 0$. However, in this frame of reference considering the distribution over the entire cloud, one would anticipate very little variation from realization to realization.

Now consider center-of-mass co-ordinates for each cloud [Bat51, CS79]. With $\kappa = 0$ take a ray passing through such a cloud at a fixed distance from the center-of-mass and analyze the concentration record in terms of expected mass fraction (replacing distance with time as the independent coordinate used in the current study). There

will be very large variations along each ray and from ray to ray for different clouds in the concentration records, and hence in the expected mass fraction. Of course with $\kappa = 0$ all of the mass is found at concentration θ_0 and the variation is in the amount of mass at concentration θ_0 found in different realizations. It is likely that larger amounts of mass will be contained in a ray passing through the center of the cloud than at the periphery.

Next consider, retaining $\kappa = 0$, the record one observes (as in the natural reference frame used in this study) as a cloud passes a fixed point in space. Large scale turbulent motions, far larger than the cloud size, could convect the cloud such that it did not pass the probe at all (meandering phenomena) or one could have a realization in which the probe passed through the instantaneous cloud center of mass. In the first case you have zero concentration and in the second close to the maximum amount of contaminant experienced at θ_0. Thus, in the hypothetical case, without any change in concentration distribution, one expects very large variations to occur, principally because a spatial reference (the fixed observation point) has been introduced.

Now consider the real case in which $\kappa \neq 0$. Because of the differing histories of fluid particles that arrive at the probe there will be an additional variation in the fraction of these that have concentrations within a delimited range.

It should be noted that, from an experimental observational point of view, in an inertial or fixed reference frame a passive scalar is moved about by the largest scales of turbulent motion [Bat49]. For a slowly changing environment one has a problem in that the effects one is trying to observe require sampling epochs that are long with respect to the time scales of this motion. That is, the time required to perform repeated trials will be relatively long. Hence there is a premium, cited in Chapter 1, placed on statistical measures that converge with relatively few realizations.

Variation can also occur due to a non-ideal continuum scale resolution probe. This will be illustrated in Sectic 4.3.

4.2 Estimate of the Variability

The value of a prediction depends not just on the prediction itself but also on knowing how reliable the prediction is. In the case at hand, this corresponds to knowing both the average concentration and the variability of the concentration. Ideally you would know the entire probability distribution function, but as a first estimate the mean and standard deviation are very useful. It seems reasonable to assume (without further support) that the variance in a bin is proportional to the expected number of sample points in a bin. Averaging data, the standard deviation of the estimated average then is proportional to $\sqrt{N}/N = 1/\sqrt{N}$, or inversely proportional to the square root of the number of data points.

One can see from the physical reasons for variability that the number of fluid elements with concentrations within a prescribed range in any realization will depend on a large number of almost independent factors. The distribution of number of elements within a bin could be viewed as binomially distributed such that the variance is proportional to the number of elements within a bin.

Turning now to the data, the same dosage can come from long exposure to low concentrations or short exposure to high concentrations. If the effective number of "exposure points" or samples is independent this suggests that the variance should be proportional to d_i/θ_i, the dosage in the bin divided by the average concentration in the bin, representing the number of points in the bin, so the variance in the mass fraction, $\hat{M}_2$, should be

$$\hat{M}_2 \propto (d_i/\theta_i)\theta_i^2 = d_i\theta_i, \tag{35}$$

or the intensity, the ratio of standard deviation to mean, should be proportional to $\sqrt{d_i/\theta_i}$. Also, the variance of the estimate should be inversely proportional to the number of trials performed, 50 or 100. Figure 11 compares the measurement to

$$d_i\theta_i/N_{\text{trials}}, \tag{36}$$

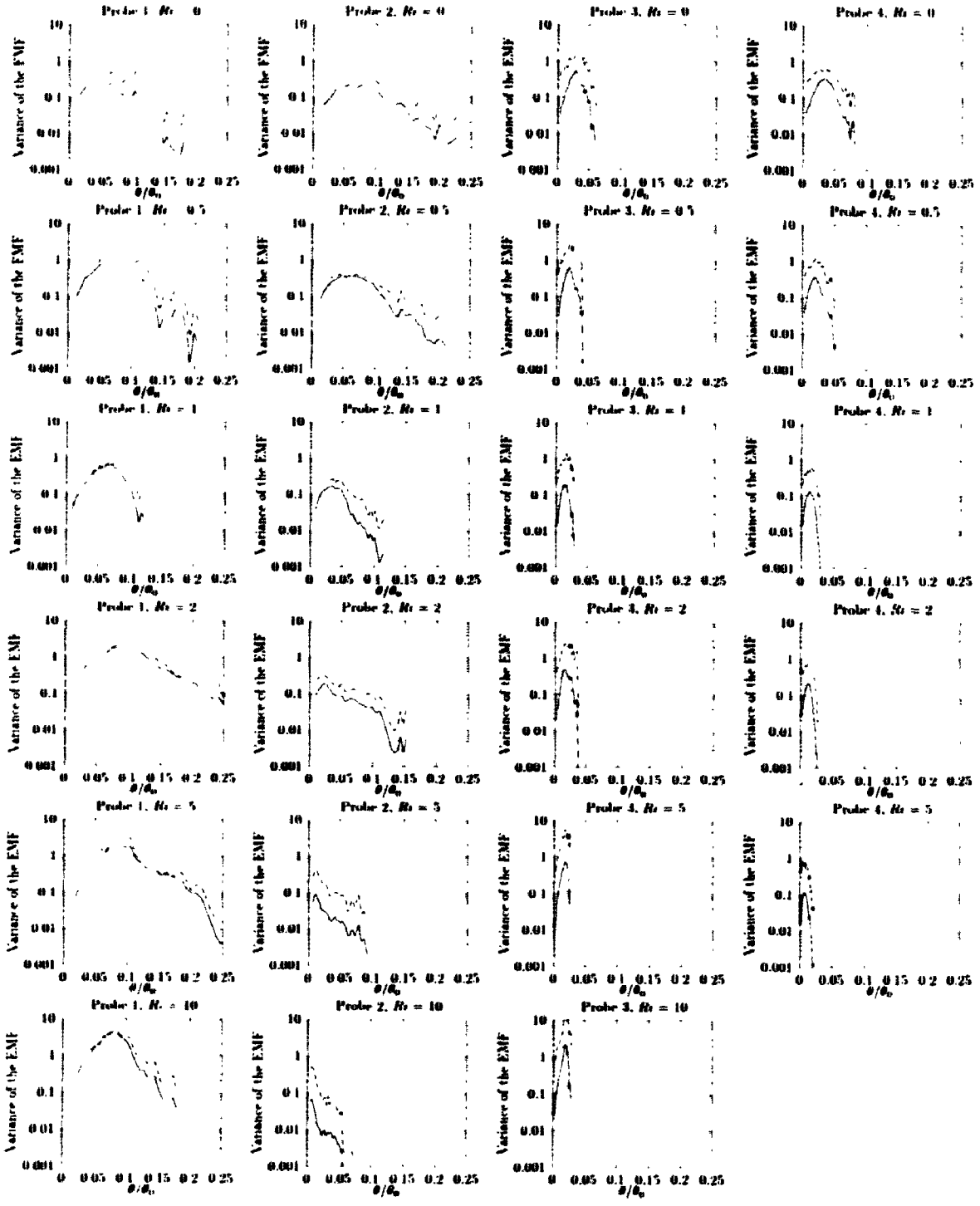

Figure 11: Observed (solid line) and predicted (dashed line) variance of the EMF.

where N_{trials} is the number of trials for a given test, as listed in Table 1.

Without any proportionality constant, the agreement between the observations and equation (36) is quite remarkable. This suggests that, especially for the lower probes, probes 1 and 3, the mass fraction in the bins behaves almost independently. For the upper probes, 2 and 4, the predicted variance is higher than the observed variance. This suggests that meandering of the cloud has a stronger effect here, with all the bins seeing more correlation in occurrence of events. It also suggests that the formula may give a conservative estimate of the variability of the EMF, making it very useful for assessing risk.

Further experimentation is required to validate and refine this formula. As the next section emphasizes, in particular probe resolution and measurement characteristics require further investigation.

4.3 Variation due to Sample Volume Geometry

We consider the case of a cloud of contaminant released instantaneously into a turbulent flow. In one realization the instantaneous continuum-resolved concentration at time t and position $\mathbf{x}$ in the coordinate system of the fixed sample volume is $\Gamma(\mathbf{x}, t)$. The probability density function $p(\theta; \mathbf{x}, t)$ describes the distribution of contaminant,

$$p(\theta; \mathbf{x}, t)d\theta = \text{prob}\left\{\theta < \Gamma(\mathbf{x}, t) \leq \theta + d\theta\right\}. \tag{37}$$

Instead of looking at the entire cloud we consider only a fixed volume V, for instance a cylinder oriented with its axis in the direction of the mean flow representing the volume which would pass through a sample plane of area A.

The probability density function (37) has integral moments,

$$M_n(\mathbf{x}, t) = \int_0^\infty \theta^n p(\theta; \mathbf{x}, t)d\theta, \tag{38}$$

such that $M_0(\mathbf{x},t) = 1$ at every point $\mathbf{x}$. The total moments are defined as,

$$M'_n(t;V) = \int_V M_n(\mathbf{x},t)dv,\ n > 0, \tag{39}$$

where the V designation indicates integration over the volume of interest. Since this volume is not necessarily finite the integral is defined only for $n > 0$ since

$$\begin{aligned} M'_0(t;V) &= \int_V M_0(\mathbf{x},t)\,dv & (40)\\ &= \int_V \int_0^\infty \theta^0 p(\theta;\mathbf{x},t)\,d\theta\,dv & (41)\\ &= \int_V 1\,dv & (42) \end{aligned}$$

which diverges if the volume V is not finite.

From equation (38), $M_1(\mathbf{x},t)$ describes the average density of contaminant at a point, so that (from equation (39)) $M'_1(t;V) = Q(t;V)$, the average mass of contaminant in the volume. Because we do not consider the entire cloud, $Q(t;V)$ is variable, subject to convection into and out of the sample volume. In contrast, for the case of the cloud-average where V = all space, $M'_1(t;V)$ describes the entire contaminant mass, which is constant by assumption.

Define the total distribution,

$$p'(\theta,t;V) = \int_V p(\theta;\mathbf{x},t)dv, \tag{43}$$

such that the integral moments of (43) for $n > 0$ are,

$$\begin{aligned} \int_0^\infty \theta^n\, p'(\theta,t;V)d\theta &= \int_V dv \int_0^\infty d\theta\,\theta^n\, p(\theta;\mathbf{x},t)\\ &= \int_V M_n(\mathbf{x},t)dv\\ &= M'_n(t;V). \end{aligned}$$

Here we are concerned with,

$$\hat{p}(\theta,t;V) = \frac{\theta p'(\theta,t;V)}{Q(t;V)}, \tag{44}$$

which is designated as the expected mass fraction. Note that

$$\int_0^\infty \hat{p}(\theta, t; V)d\theta = \frac{1}{Q(t; V)} \int_V dv \int_0^\infty d\theta\, \theta\, p(\theta; \mathbf{x}, t) = 1, \tag{45}$$

and that the total moments defined in equation (39) are simply related to the moments of $\hat{p}(\theta, t; V)$,

$$\hat{M}_n(t; V) = \int_0^\infty \theta^n\, \hat{p}(\theta, t; V)d\theta, \tag{46}$$

by,

$$M'_{n+1}(t; V)/Q(t; V) = \hat{M}_n(t; V). \tag{47}$$

From the measurement or prediction of $M_n(t; V)$ one can in principle recover $\hat{p}(\theta, t; V)$ using equation (46) (see [DS90]). The idea is that prediction of integrated statistics such as $M_n(t; V)$ and the direct measurement of $\hat{p}(\theta, t; V)$ should be more straightforward than measurement of distributed properties such as $p(\theta; \mathbf{x}, t)$, and should be more applicable in complex environmental flows.

The definition (44) has the interpretation that $\hat{p}(\theta, t)d\theta$ is the expected mass fraction in the sample volume V that is found in the concentration range θ to $\theta + d\theta$ in the volume at time t. The median concentration $\theta_{1/2}(t)$ defined by,

$$\int_0^{\theta_{1/2}} \hat{p}(\theta, t)d\theta = 1/2, \tag{48}$$

should be a good approximation to the median described in [CS77].

4.3.1 Model

The interpretation given in [CS90b] is that the distribution of contaminant within a cloud is that of strands or sheets of relatively high concentration with a width or thickness comparable with the conduction cut-off length, embedded in an ambient of relatively low concentration. That interpretation is supported by experimental observation [BC92].

We consider a dosage model based on the assumption that the contaminant is concentrated in thin straight strands and that the dosage, as discussed in Chapter 1 is the total mass inside a cylinder of radius R and infinite length. This might approximate, for instance, the exposure of a person standing still as a cloud of contaminant drifted past, exposing the person to a longitudinal sampling of the cloud.

Suppose that a single straight strand of negligible thickness and uniform mass per unit length ρ intersects the cylinder at some point. Let the distance of closest approach between the strand and the axis of the cylinder be r. The assumption that the strand is straight is consistent with the "sheets and strands" model of turbulent dissipation. We observe that the strands have a large radius of curvature compared to their thickness [DSB91]. We extend this to the assumption that the radius of the sample volume is small compared to the typical radius of curvature of the strands. This is consistent with other approximations we make here, as what we are considering is a mechanism through which the measured variability may be quite dependent on the shape of the sample, and not just the size of the sample.

Assume that the strands are uniformly distributed in space both as to position and orientation in the neighbourhood of the sample volume, so that, given an intersection with the cylinder, the strand is randomly located on a cross-section. Then,

$$p_r(r)dr = \frac{2\pi r}{\pi R^2}dr, \quad 0 \le r \le R, \tag{49}$$

the probability that the observed strand will cross between r and $r + dr$ from the axis.

Similarly the angle to the plane normal to the axis, α, is randomly distributed over a hemisphere so,

$$p_\alpha(\alpha) = \cos(\alpha), \quad 0 \le \alpha \le \pi/2. \tag{50}$$

Then $\Gamma = \rho l$, where ρ is the uniform strand density and l is the length of strand within the cylinder. For radius r and angle to the $x - y$ plane α, $l = 2\sqrt{R^2 - r^2}/\cos(\alpha)$, so

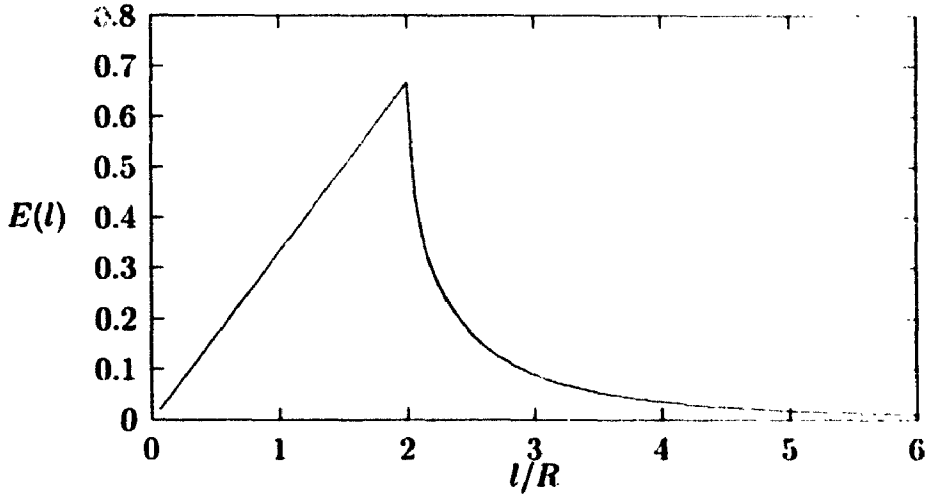

Figure 12: Mass Fraction versus Concentration

$\Gamma(r,\alpha) = \rho l = 2\rho\sqrt{R^2 - r^2}/\cos(\alpha)$. Then $p(\theta)d\theta =$ prob $\{\theta < \Gamma(r,\alpha) < \theta + d\theta\}$.

We can calculate the total moments,

$$\int_0^\infty p_n(\theta)d\theta = \int_0^{\pi/2} d\alpha \int_0^R dr\, p(r)p(\alpha)\Gamma^n(r,\alpha). \tag{51}$$

From $n = 1$, the first moment, the mean mass in the cylinder is $\bar{\theta} = 2/3\pi\rho R \approx 2.09\rho R$. The second moment is unbounded. This comes from non-physical aspects of the model – the infinitely long strand lining up along the axis of the cylinder. However the model is sufficiently realistic to suggest that the real situation would produce a very large sample variation and results would converge very slowly. Large numbers of samples might be required just to establish the mean. And recall that this model assumed that exactly one strand intersected the cylinder. A random number of intersections could add to the measurement difficulty.

Finally consider the distribution of mass with concentration. For any concentration θ we determine that $l = \theta/\rho$. Since $l = 2\sqrt{R^2 - r^2}/\cos(\theta)$ we can look at the

probability of l as,

$$E(l) = \int p_r(r(l))\, p_\alpha(\alpha)\, dr(l) d\alpha. \tag{52}$$

This is plotted in Figure 12. It represents the amount of contaminant in V. The peak in the curve occurs when the length of strand equals the diameter of the cylinder. For longer lengths of strand not all orientations permit the strand to fit into the cylinder so the frequency of occurrence decreases. Normally we would consider this as a function of the x and y coordinates of the cylinder (a projection along the z-axis) so that the density would be $\rho l/A$. This of course assumes exactly one strand, so the strand density also needs to be taken into account. If we assume a density low enough that at most one strand is likely to intersect the cylinder at a time then $E(l) \times \rho \times$ strand density = the area density function of contaminant. The effects of multiple strands can also be taken into account with some additional calculation, although we might need to consider multistrand correlations for the analysis to be significant.

4.3.2 Conclusion

We have developed a variation on the idea of a "cloud-average" dilution probability. A simple model for the structure of contaminant predicts high variability of measurements of dosage. We also calculated the dosage-average dilution probability function for this model. When the sample volume is small this model corresponds to the measurement resolution problem.

4.4 Trends in the Evolution of the EMF

4.4.1 Batchelor's analysis of average cloud shape

The WSL data should compare well with existing theories about the behavior of the "mean" behavior, the downstream development of the cloud, including speed of the center of mass of the distribution and the spread of the cloud. One Lagrangian model of this development comes from G.K. Batchelor [Bat64], which summarizes an analysis of the development of a release at the surface in a typical atmospheric flow, with neutral stratification and a constant-stress "logarithmic" layer near the surface. The details of the model do not matter too much. While derived in the context of a logarithmic profile, they could give an adequate approximation for similar situations, to the accuracy to which dispersion models can aspire at the present time. The key points for this study include the following. A surface release develops in a geometrically similar way, with the shape remaining constant and the linear dimensions growing linearly in time. Approximate values for the spread of the cloud used by Batchelor [Bat64] come from early experimental data. The WSL data should agree with this model. Raised sources behave the same way as surface sources upstream some distance, at a "virtual origin". The model applies only asymptotically, since the WSL experiment uses a source of dimensions (especially height) large compared to the distance downstream to the sampling points. The height of the release cylinder, 13cm, is large compared to the vertical spread during the time for the released gas to move downstream to the sampling points. Similarly, the horizontal spread cannot fully develop. However, we observe a good agreement, which supports the robustness of the cloud model.

The comparison of theory and experiment provides some insight. If the Batchelor model applies then the density of the cloud will decrease with the increasing volume and hence will be proportional to $1/t^3$. Any function of position and concentration

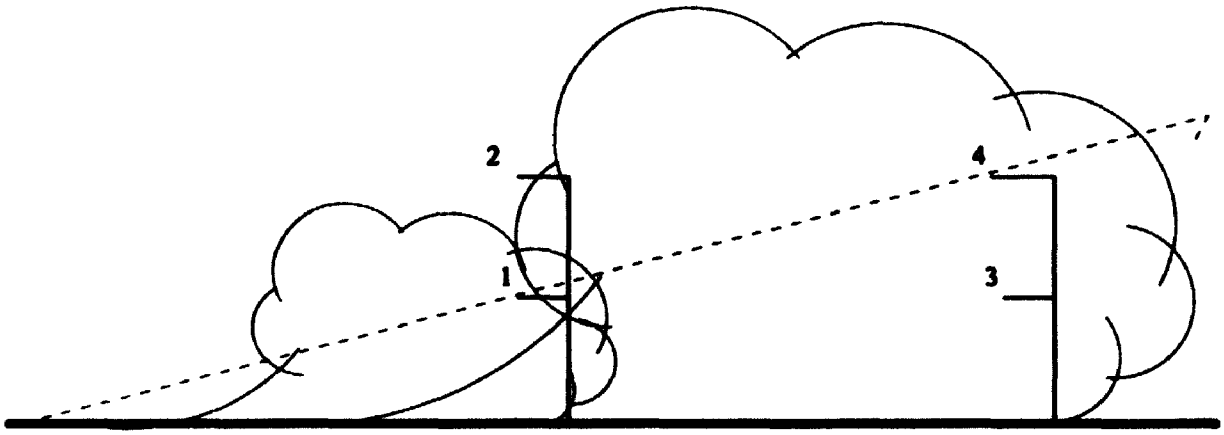

Figure 13: Equivalent probe trajectories through cloud

in the cloud should then have the form $f(\mathbf{x}_R/t, C_R/t^3)$ where $\mathbf{x}_R$ is the equivalent position at reference time t_R, and C_R the corresponding concentration. Thus if the original time series data are multiplied by $(t + t_V)^3$, where t_V is a time offset corresponding to the virtual origin offset, then the probe located at x_P at time t_R would correspond to a probe at $x_P t_P/(t + t_V)$ at any other time t. If we consider the cloud at time t_R then Figure 13 shows that the measurements correspond to measurements at time $t = t_R$ along radial trajectories from the virtual origin. With such an analysis, the time histories from upstream and downstream probes can be compared.

The data was transformed as follows. If L_0 is the distance upstream from the release point to the virtual origin, and u is the reference wind speed (at a height of 13cm) then the transformed time t_n becomes

$$t_n = t + L_0/u. \tag{53}$$

If the distance from the release point to the probe is x_P then the distance coordinate which replaces the time coordinate in the original data is

$$x_n = \frac{L_0 + x_P}{u t_n}. \tag{54}$$

The concentration is scaled by t_n^3:

$$\theta_n = \theta t_n^3. \tag{55}$$

Then $\hat{p}_n(\theta_n)$ is calculated the same way as $\hat{p}(\theta; \mathbf{x})$ with x_n replacing time t as the independent variable, to give the expected mass fraction as a function of θ_n along the ray passing through the origin and through the sampling point.

As Figure 13 suggests, the trajectories for the probes 1 and 3 are fairly close together. By adjusting the virtual origin we can get a near match on these two profiles, as shown in Figures 14, 15 and 16. The virtual origin for release appears to correspond to a distance upstream of about 5m. The corresponding time can be scaled from the mean velocity at the height of the cylinder, the standard reference speed used in the experiment. With this origin, the mean time history for each data set collapses reasonably well as shown in Figures 14, 15 and 16. Discrepancies clearly show the effects of time development, as the cloud moves downstream. Clearly, the measurement points are not "far" downstream, and the cloud has not reached a fully self-similar state. On the other hand, the assumption of t^3 development does result in the data collapsing quite well, with the upstream and downstream profiles overlapping in a consistent fashion.

Each measurement point corresponds to a traverse along a line radiating from the release point. As Figure 13 shows, the intermediate traverses by probes 1 and 4 should produce results between the extreme probes 2 and 3. And Figures 14, 15 and 16 do show this agreement. The general agreement of the central profiles confirms the use of 5m as an appropriate virtual origin, and the t^3 development of the cloud. The differences between these two profiles show the development of the cloud towards an asymptotic state as it progresses downstream, starting from a release point much closer than the virtual origin. Informal comparisons showed that the cubic time development much better characterizes the cloud behavior than either quadratic or linear time dependence, although due to the proximity of the large source to the measurement points, either of those alternatives could have been plausible.

When dealing with the time histories (as compared to the EMF which we will

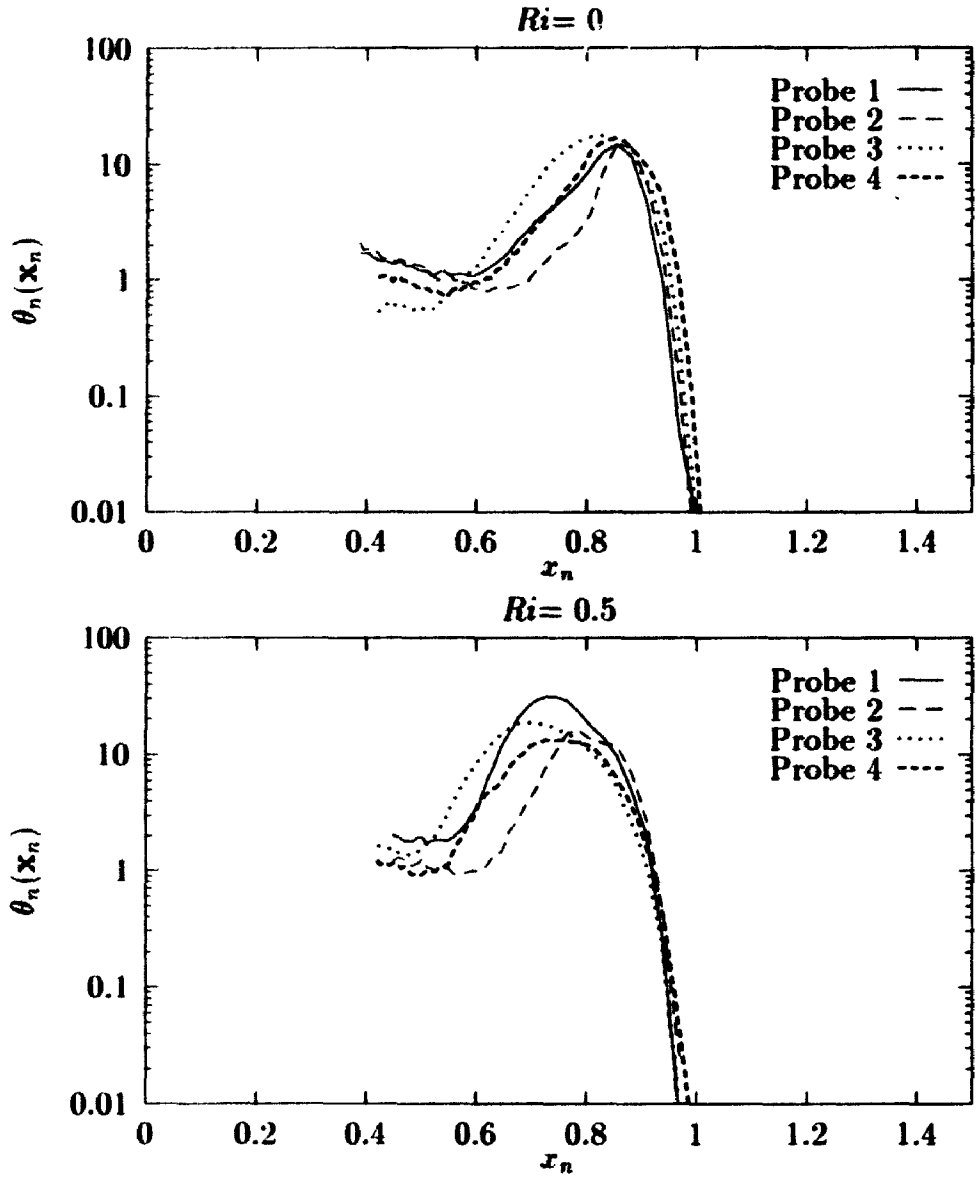

Figure 14: Collapse of measurements from all four probe positions for $R_i = 0, 0.5$.

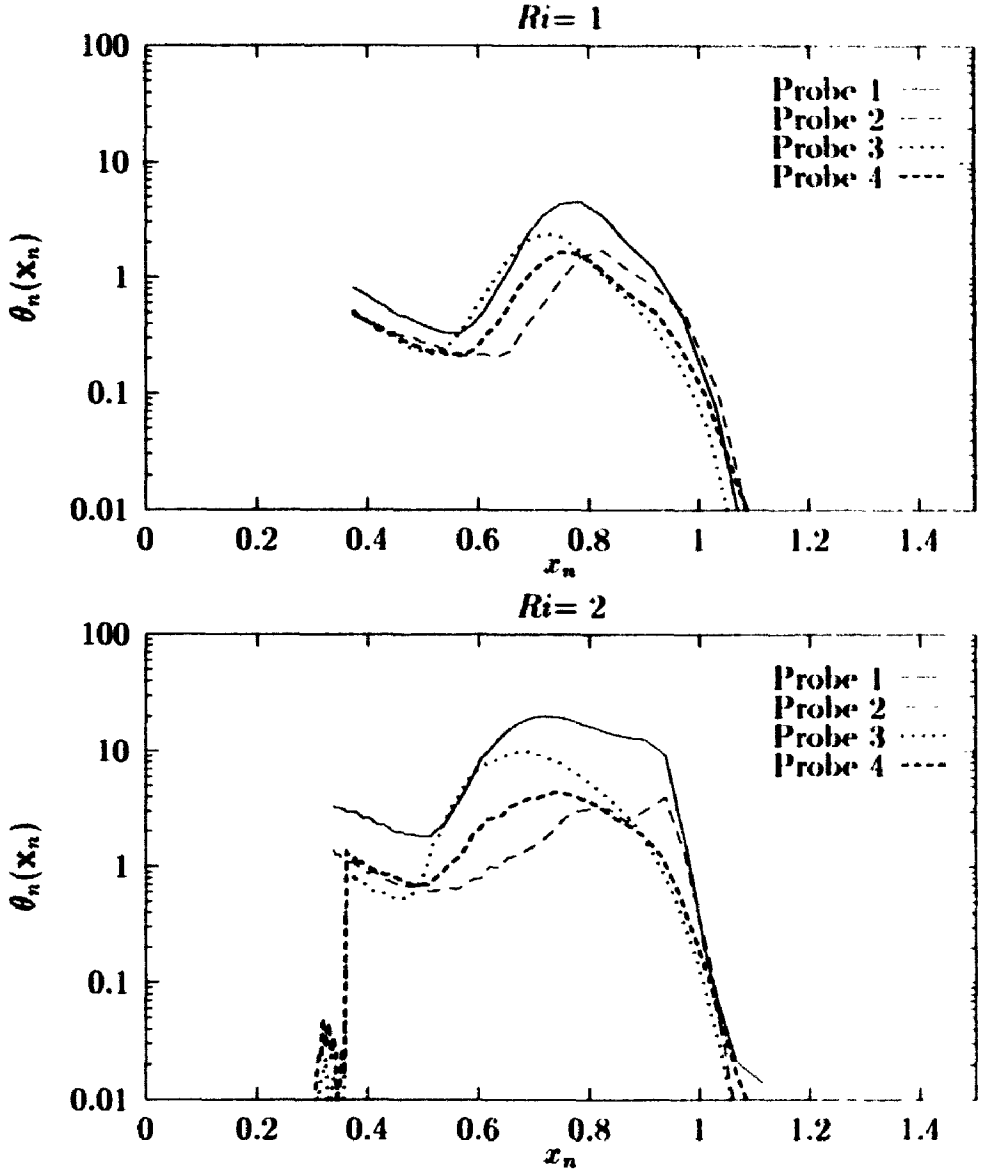

Figure 15: Collapse of measurements from all four probe positions for $R_i = 1, 2$.

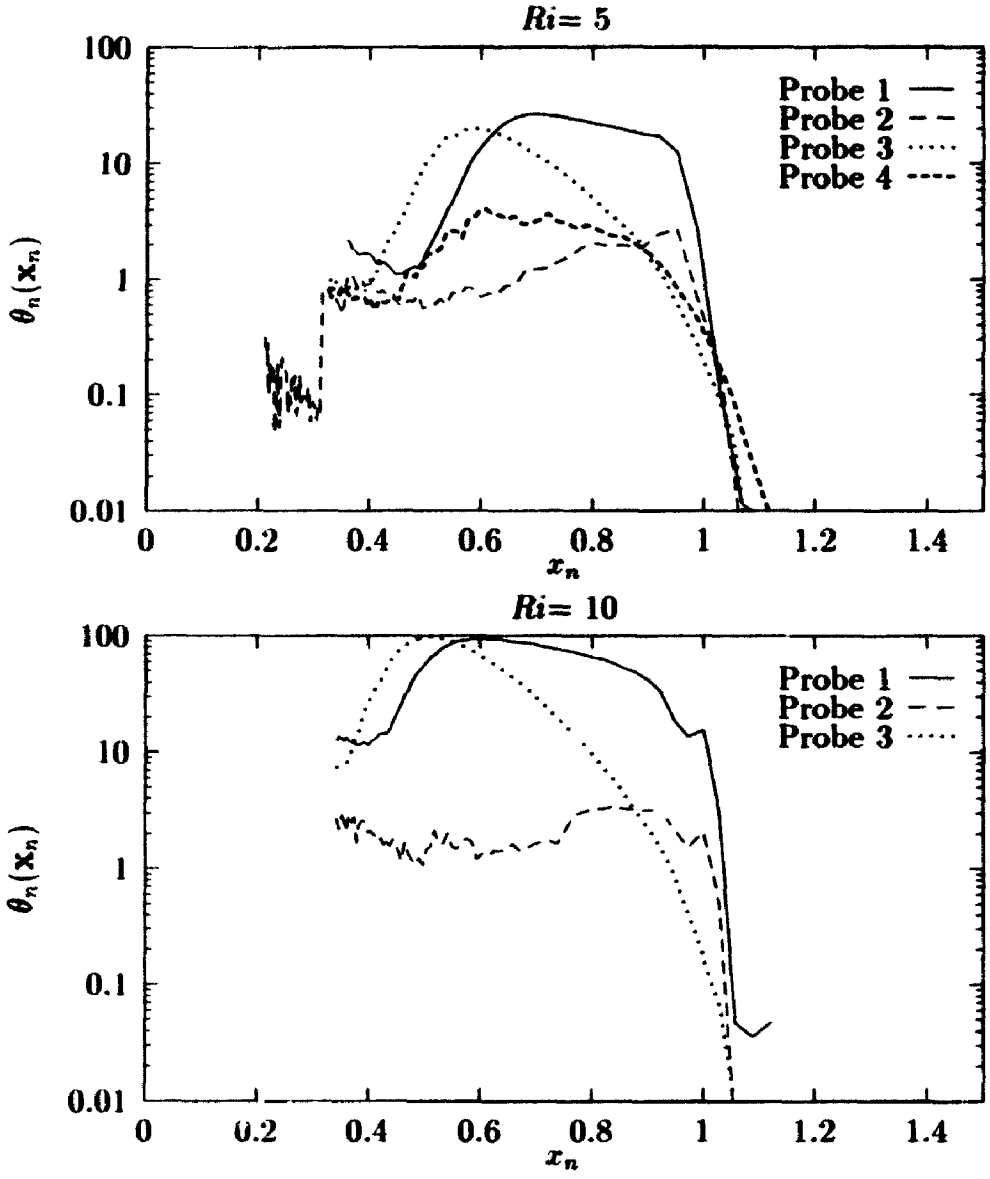

Figure 16: Collapse of measurements from all four probe positions for $R_i = 5$, 10.

consider next), the primary difference between the upstream and downstream probe positions is found near the leading edge of the cloud. This part of the flow has the least time to develop after release before reaching the closer probes, and hence should show the most change between the two probe positions. The trailing part of the cloud reflects entrainment of the contaminant, and has much more time for self-similar development, so the better agreement is not surprising.

The above analysis can apply only to the ensemble-mean behavior of the cloud, not the variability expected in a given release. Greater analysis is not justified for the present study. However, presumably a treatment of the release as an ensemble of spatially distributed point releases, instead of the treatment with a virtual origin, would produce even better agreement between experiment and theory.

4.4.2 EMF and t^3

The spatial analysis works well enough to justify repeating the analysis for the EMF, first normalizing each time series with the cube of the time since the "virtual release". This normalization does not commute with the EMF computation, since it affects the sorting of the data points, with small late points becoming much larger after normalization compared to earlier points, as shown in Figures 14, 15 and 16. Because of this, considering experimental noise and similar factors, we did not expect that the data would collapse as well as the time histories did. However, proceeding, as Figures 17, 18 and 19 shows, we do get reasonable collapse of the data

In conclusion, results of this analysis are very encouraging, but far more experimental evidence from cloud studies is required.

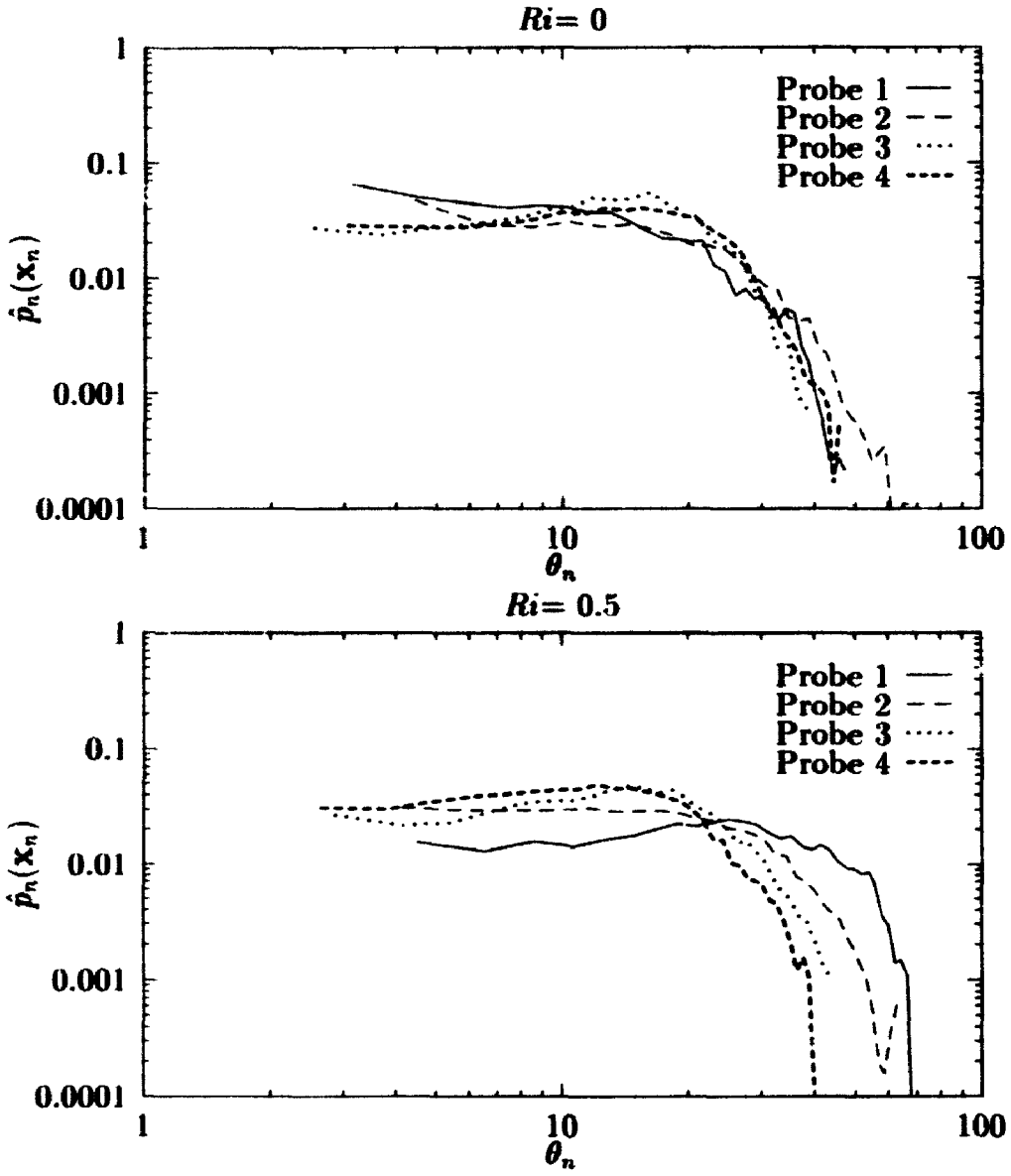

Figure 17: Collapse of normalized EMF from all four probe positions for $R_i = 0, 0.5$.

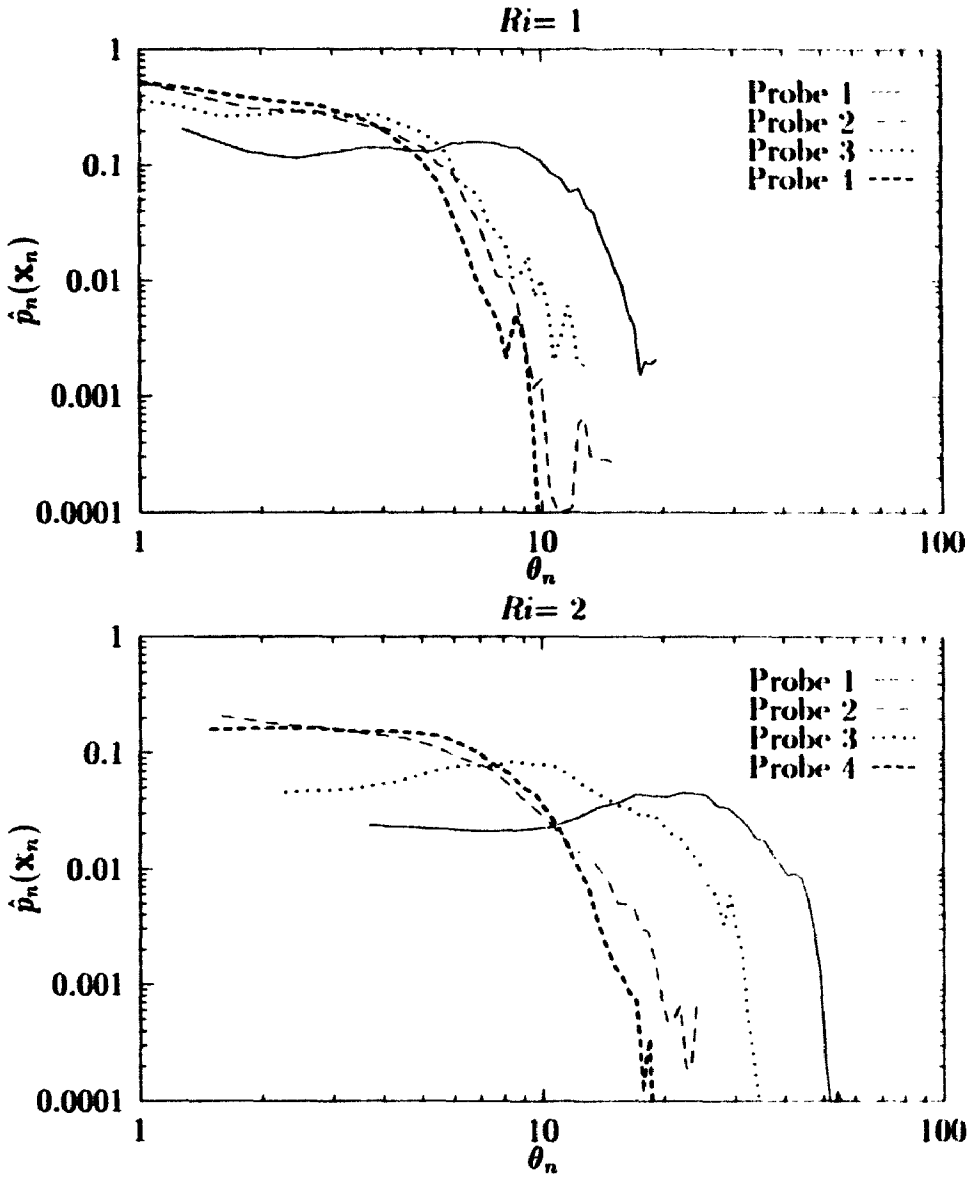

Figure 18: Collapse of normalized EMF from all four probe positions for $R_i = 1, 2$.

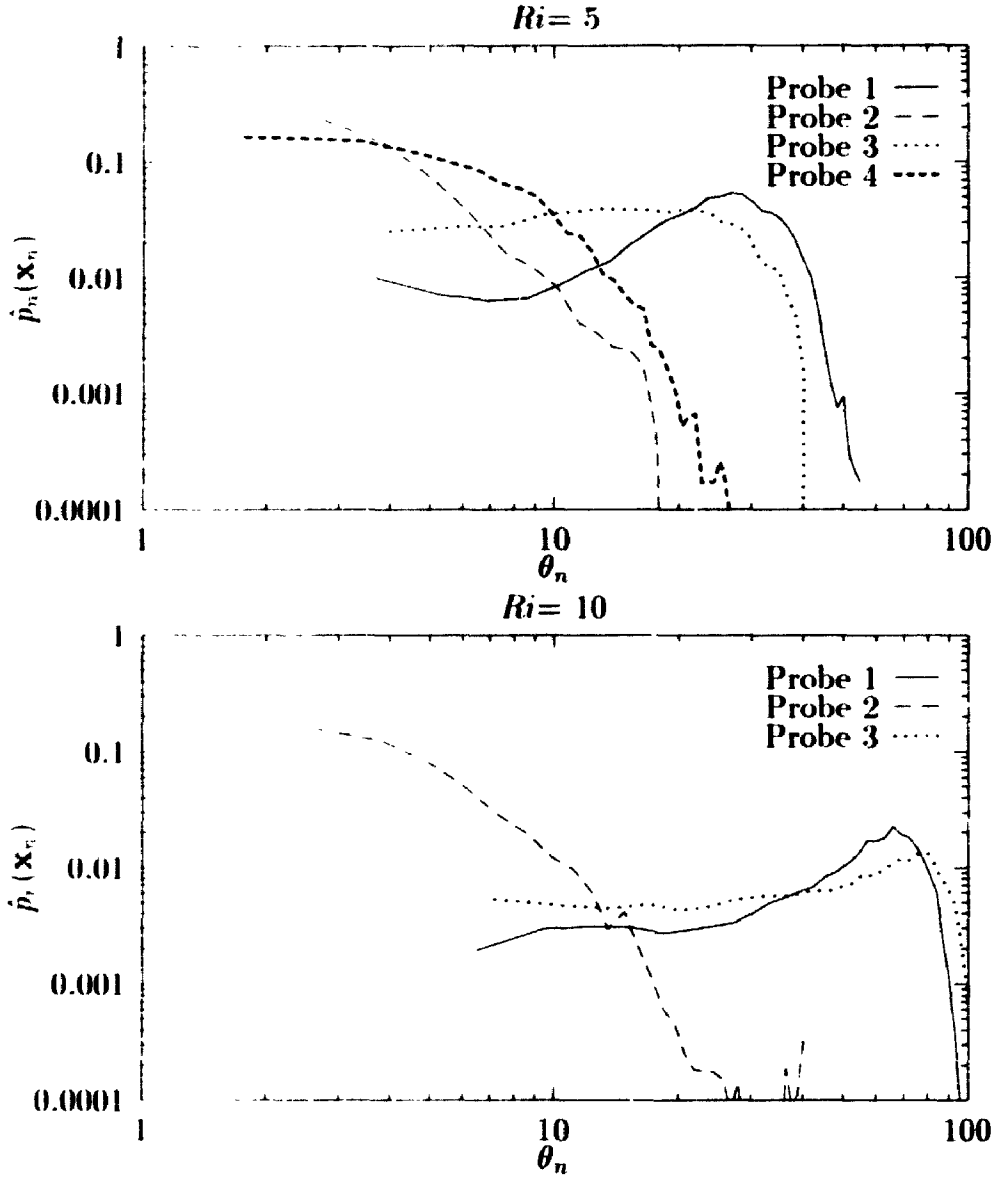

Figure 19: Collapse of normalized EMF from all four probe positions for $R_i = 5, 10$.

4.4.3 Evidence for an α-β Description

There are no distributed measurements for moments in a cloud with which to validate the α-β model. A recent paper by Mole and Clark [MC94] has made a very significant contribution in this regard. They showed that the manipulation of equation (25) leads to the parameter-free relationship between kurtosis k and skewness s

$$k = s^2 + 1. \tag{56}$$

They further showed that this was a lower bound corresponding to a two-state process. For all other processes,

$$k \geq s^2 + 1. \tag{57}$$

Their validation with field data for a continuous plume was convincing, with data points lying somewhat above the curve given by equation (56). Figures 20, 21, and 22 plot this relationship for all WSL tests.

The α-β description of equation (25) is presented in its simplest form using values from Table 4 of [CS90b] to suggest β is independent of the moment order n. Recently it was shown numerically [DSY94] and analytically [SY94] that the use of one α and one β value in equation (25) leads to a two-delta-function probability density function. It has been further shown [SY94] that a Gaussian convolution function with a very small and virtually constant non-dimensional variance can be used with this two-delta-function probability function to reproduce the observed probability density functions in a respectable range of experimental flows. This is compatible with a simple model focussing on the sheet-strand like texture of a turbulent contaminant field [LSY94] which appears to recover a considerable amount of what is observed in a grid-generated turbulent plume from a continuous point source or a continuous line source. This model agrees with the convolution function in that a Gaussian distribution of strand and background concentration values gives a Gaussian convolution with the two-delta-function solution from a causal model with a nonzero background

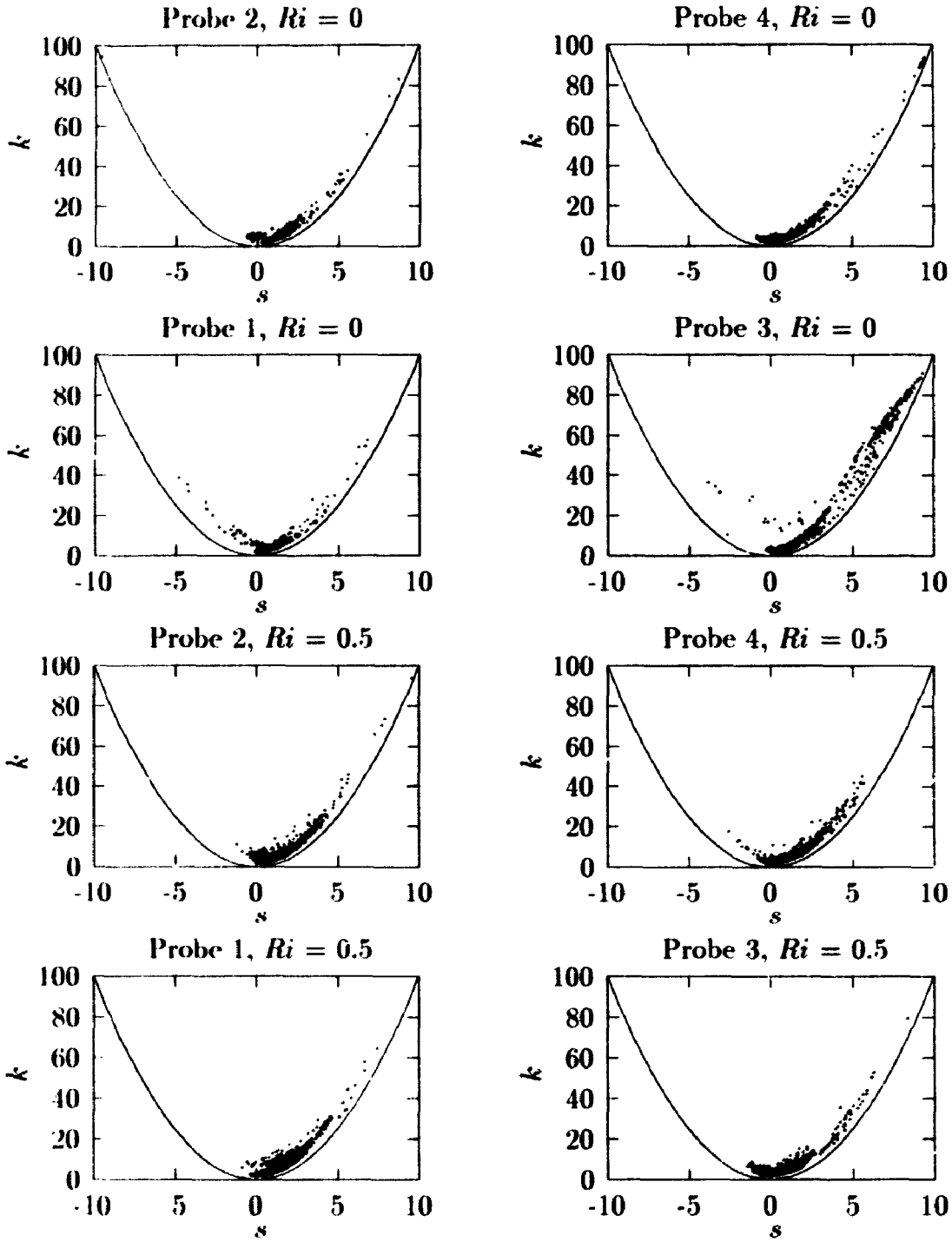

Figure 20: s *vs* k, with reference curve $s = k^2 + 1$, for Richardson numbers 0 and 0.5.

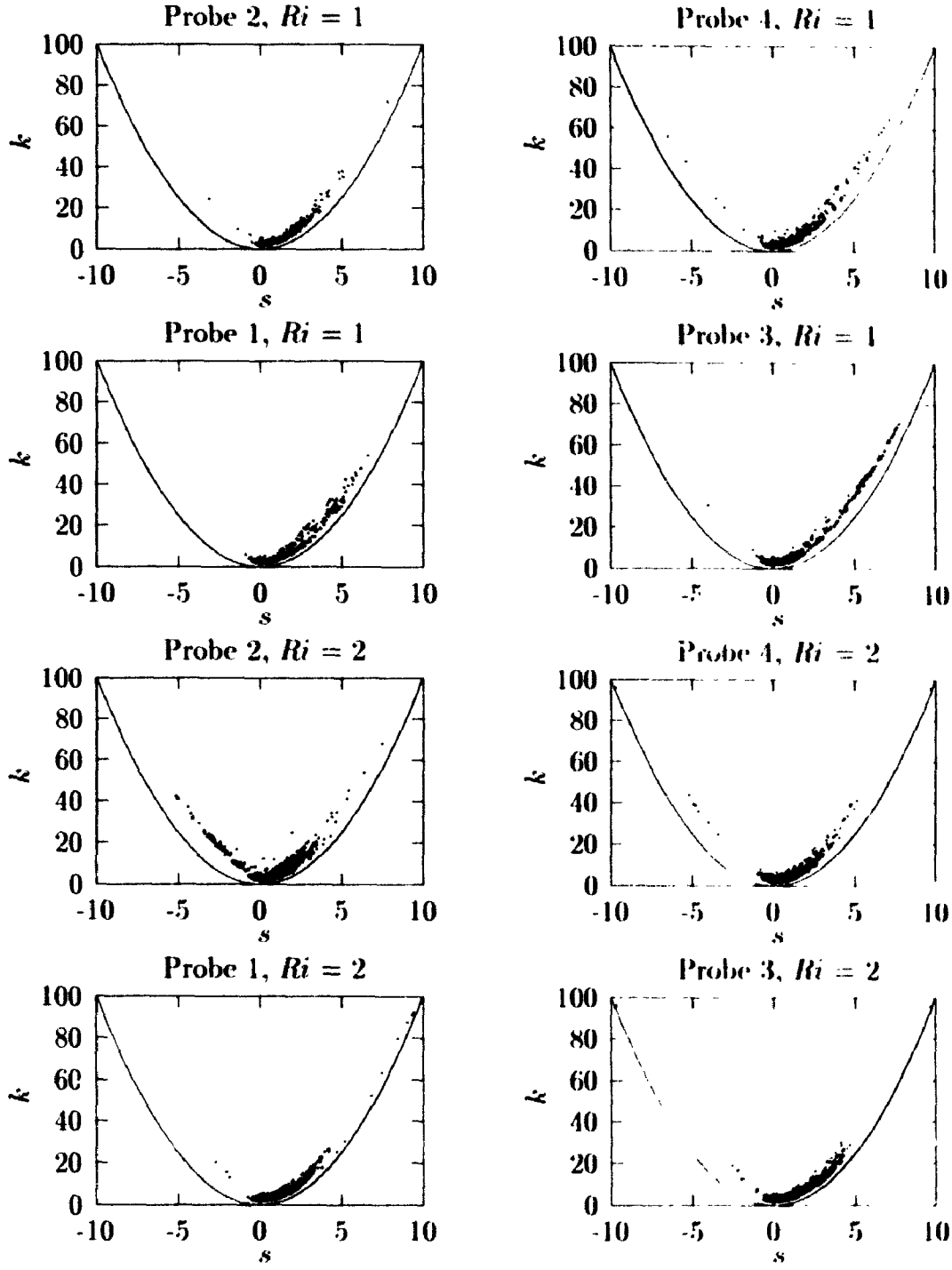

Figure 21: s *vs* k, with reference curve $s = k^2 + 1$, for Richardson numbers 1 and 2.

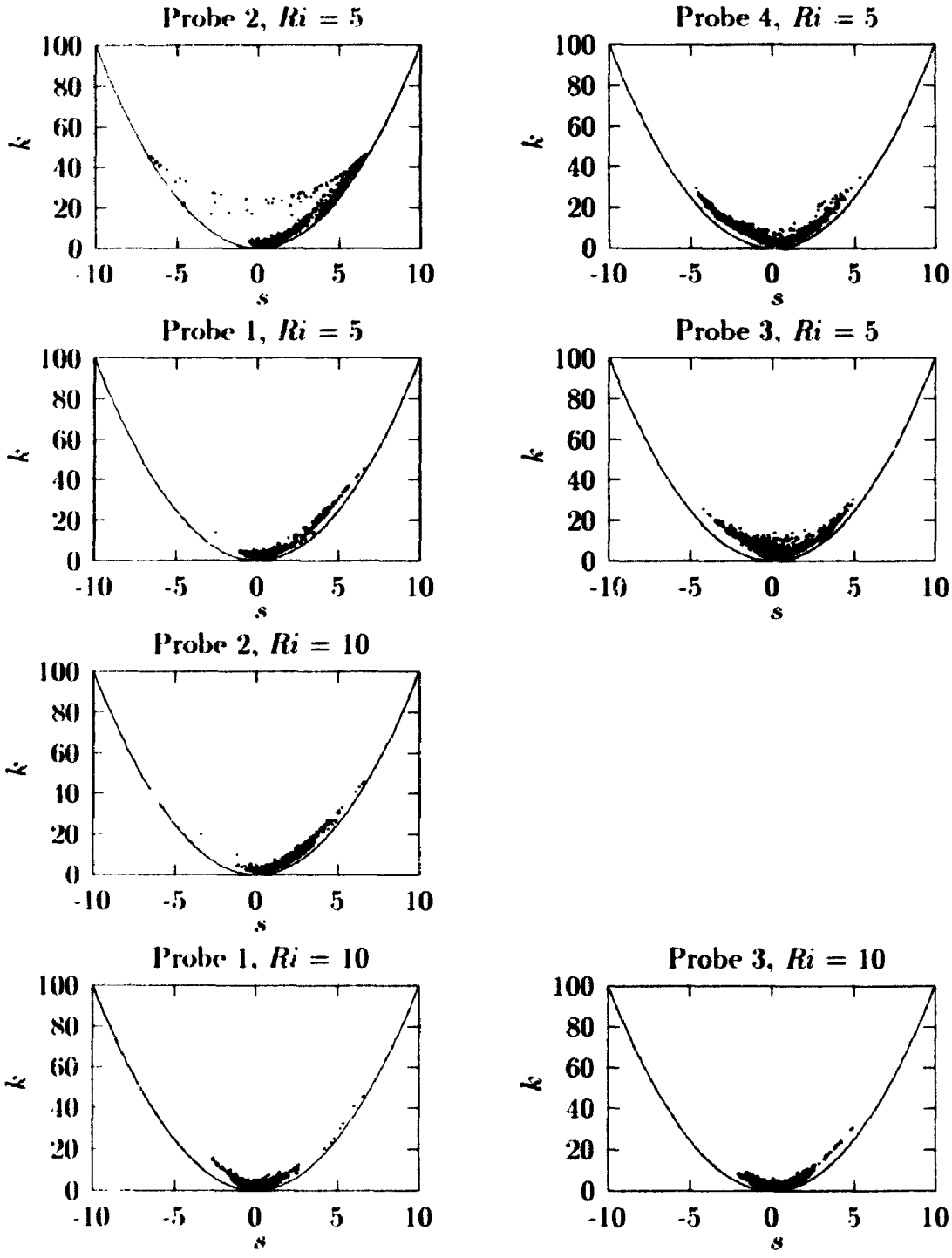

Figure 22: s *vs* k, with reference curve $s = k^2 + 1$, for Richardson numbers 5 and 10.

concentration and a strand concentration distribution. This result is also consistent with the observed data points occurring slightly above the curve given by (56).

We note also that the effects of experimental resolution or noise and of a legitimate distribution of strand concentration values say, could be indistinguishable, as Section 4.3 shows.

Most significantly here, this result, using sampling points in isolation rather than a complete cloud analysis, allows one to test the proximity to an α-β description. Thus the curves shown in Figures 14, 15 and 16 suggest, considering the experimental noise, that the α-β prescription may well provide a good approximation to both dense and neutrally buoyant clouds. This then opens the door to the predictive procedure described in Chapter 2. The modification introduced above would result in a slight adjustment in the simple example calculations done in Section 2.4 and mainly in the low concentration values.

Chapter 5

Problem Assessment and Directions for Future Progress

It is appropriate, now that the problem of the dilution of a contaminant cloud is introduced and a new probabilistic measure, the expected mass fraction, developed and explored to attempt to assess this contribution in the context of environmental problems.

5.1 Importance of the Problem and State of the Art

In a paper by Dayal and Trieff [DT92] at an *Environmetrics* conference in Helsinki in 1992, experimental data presented consisted of the number of people admitted to regional hospitals as a result the accidental release from an oil refinery of more han forty thousand pounds of highly corrosive and toxic hydrofluoric acid. Based on a standard Industrial Source Complex (ISC) algorithm they stated that safety directions led to people migrating from safe to hazardous regions in some cases. In conclusion they stated that "these observations suggest severe limitations of mathematical models in

predicting individual exposures."

Contini *et al* [CAZ90] discussed the need for much more work on all phases of risk assessment for releases of toxic gas. This followed a benchmark study by 11 teams from 26 European organizations comparing analysis of the same (hypothetical) industrial scenario. Their conclusion was that "significant discrepancies were found, essentially due to the different assumptions adopted in modelling the release and dispersion phenomenon".

Generally in these studies mean concentration values are used which do not directly relate to the dilution problem. Clearly there is a need for a reliable prediction of contaminant concentration values from the view point of assessing hazard and risk. The probability of an accident occurring must be established separately. Following that the dilution and spread of contaminant concentrations may be worked out. Then the consequences may be determined from this, through such toxicological techniques as probit analysis. Given that environmental flows are complicated such that source and flow conditions are variable and not too well defined one would ideally like a simple, reliable and credible representation. If such a representation is overly conservative exaggerated predictions could cause the economy to grind to a halt, if given credence. The challenge is to define a measure that can actually be compiled experimentally, contains relevant information, and has some prospect of theoretical prediction. The expected mass fraction contains relevant information on contaminant dilution, and is a reasonably rapidly converging measure which, as discussed, has a reasonable prospect of theoretical prediction.

5.2 Complexity

In dealing with a cloud of flammable material passing over an observer at a fixed location with a flame one is interested in the probability of ignition occurring [BBDT78].

This will occur if the flame encounters fluid with concentration values within the flammable limits (*e.g.* between 5 and 15% for methane). If there were no molecular diffusion, *i.e.* $\kappa = 0$ and the initial source concentration θ_0 was outside the flammable range there would nowhere at any time be ignition and if it was within this flammable range then any time the flame encountered source material there would be ignition. To assess the ignition probability, including the flame-over problem and determine what fraction of the cloud would ignite, for example, one would require the n-point joint probability density function of concentration in space and time where n is very large. Such a measure, although representative of the physical situation, could not be measured in practice. Far too many realizations would be required and these would take up far more time than varying conditions in any full-scale experiment would allow. The expected mass fraction is a compromise measure that can actually be measured. This does not represent the probability of encountering y units of mass over a specified concentration interval when a cloud passes a fixed point. It is the expected average outcome. As such it does give direct information on the dilution problem but one would also like to have the variability of this relatively simple measure as well. Initial analysis indicates that the variability can be estimated from the Warren Spring data set.

Another situation like the "camp fire" smoke problem arises when the military "lays down smoke" to obscure visibility; smoke particles (sometimes) can be treated as a continuum phenomenon with κ due to Brownian motion. Here it is the accumulated particles in a ray through a puff or continuous plume which are important [PHC93].

The relevance of the information contained in the expected mass fraction has much to do with the quantification of toxicological impact. In the case cited above with flammability the consequences appear to be reasonably straight-forward by comparison. No doubt the stimulus-response characteristics will vary widely over the range of different toxic stimuli. Researchers in at least 50 laboratories are currently studying

large numbers of chemicals using *in vitro* cytotoxicity tests to find ways of predicting human toxicity [SHRJ92]. The present study should provide a useful basis for application of such studies.

Kawall [Kaw93] has studied the wake behind an elevated turbulent jet in a cross-flow, and Ye [SY94] has shown that these results too match the α-β model, so that the method presented here may well apply in this case also.

The range of applicability appears extensive. The closure model of Labropulu and Sullivan [LS94] which predicts correct results for $\alpha(x)$ and $\beta(x)$ evolution in many flows, provides the prospect of expanding the applicability of the model. So also the prospects of using a simple closure [LS94] which predicts qualitatively correct results for $\alpha(x)$ and $\beta(x)$ evolution in wind tunnel plumes and self-similar shear flows including jets, wakes, mixing layers and buoyant plumes are promising. The apparent independence from source conditions that the WSL data suggests requires more verification, as a potential reduction in one important source of variability in prediction.

I hope that the work described in this thesis will provide a framework with which to design and analyze the results of many new experiments in diverse flows and contaminant release configurations. Future experiments need to concentrate on the temporal and spatial resolution of probes, and their effects on observed variability.

Appendix A

The α-β Formulation of Chatwin and Sullivan

Chatwin and Sullivan [CS90b] considered the problem of the release of a cloud of tracer gas, and considered first the hypothetical case of a release when the molecular diffusion, κ, equals zero. For this case, fluid particles retain their original concentration of tracer, either zero if they originated outside the cloud, or θ_0, the original concentration, if they originated inside the cloud. At any fixed point in space $\mathbf{x}$ at time t the concentration can then be only zero or θ_0. The probability that the concentration is θ_0 is defined as $\pi(\mathbf{x}, t)$. Then $p(\theta; \mathbf{x}, t)$, the p.d.f. of concentration, must have the form

$$p(\theta; \mathbf{x}, t) = \pi(\mathbf{x}, t)\delta(\theta - \theta_0) + (1 - \pi(\mathbf{x}, t))\delta(\theta), \tag{58}$$

with only two values of concentration possible. The moments of this distribution then are

$$m(\mathbf{x}, t) = (\theta_0 - \theta)^n + (-1)^n(\theta_0 - C)\theta^n. \tag{59}$$

Chatwin and Sullivan then argue that in the case of a real gas, when $\kappa \neq 0$, convective processes still proceed quickly compared to molecular diffusion, and the moments of the actual p.d.f. should approximate the moments of the $\kappa = 0$ case. They

hypothesize that

$$m_n(\mathbf{x}_0, t) = \beta^n(t) C_0^n(t) \left(\chi(\alpha(t) - \chi)^n + (-1)^n(\alpha(t) - \chi)\chi^n\right)/\alpha(t), \qquad (60)$$

is a plausible approximation to the moments, where $\chi = C(\mathbf{x}, t)/C_0(t)$, α and β are functions of time, but not position, as the cloud evolves, and $C_0(t)$ is the maximum concentration anywhere in the cloud at time t.

Appendix B

Note on Data Analysis

B.1 Drift Correction

The Warren Spring Laboratory data was received in digital form on computer "floppy disks". On examination, one data set, for probe 4, Richardson number 10, was not readable. Since at the time neutral gas releases were of primary interest, the missing data was considered to be of minor importance and was not replaced. Accompanying the data was a Fortran program which allowed manipulation of the data. Plotting typical data and recalculating basic statistics to compare with values already available [HWM+91] confirmed that the data (other than the missing data set) was intact and received correctly.

One of the earlier analyses performed was to look at the statistical stability available from the sets of 50 or 100 releases. One way to examine this was to look at the estimate of average dose obtained from one release, two releases, three releases, etc. Taking the samples in order from the data sets revealed that the dose estimates did not converge as expected, but showed a trend with number of releases, as shown in Figure 23 for probe 1, Richardson number 0. This was typical of other data sets also.

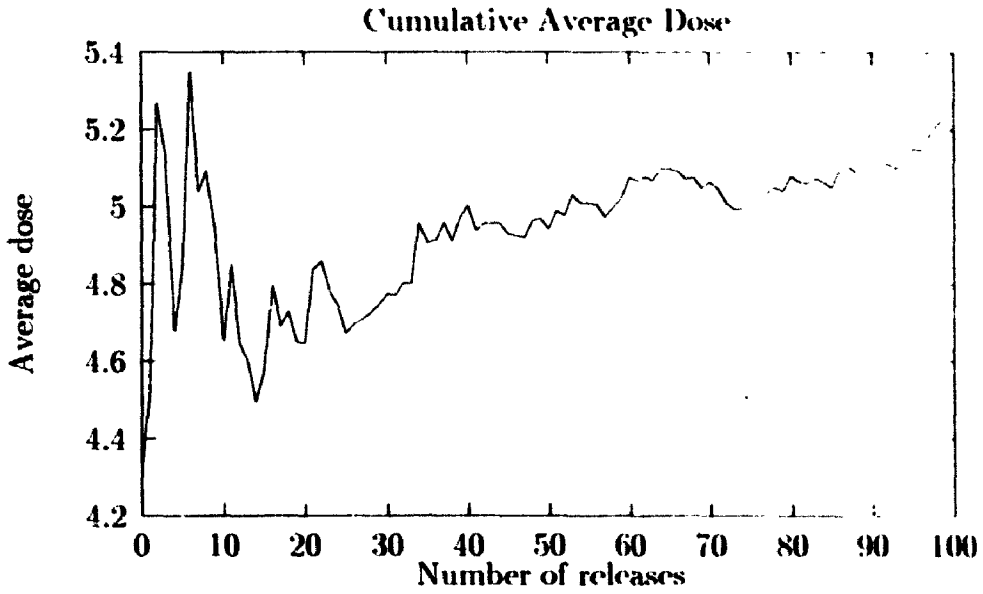

Figure 23: Drift of cumulative average of dose for probe 1, Richardson number 0, before drift adjustment.

The possibility of a simple drift in the zero reference level was eliminated by examining the early part of eaach release, before any tracer had reached the sampling probe. These values were consistently close to zero and this could not explain the observed problem. Picking the samples in random order instead of sequentially confirmed that the phenomon was not a statistical artifact. Since the effect was relatively small, and no better explanation was forthcoming, the assumption of a drift in gain, linear in time, was made and the data sets were adjusted. For each data set, a least-squares linear fit was made to the doses of each release. Picking the mid-point of the set of data as the reference, the amplitude of each release was then adjusted by multiplying the data by a constant value for each release. This assumed that the duration of each release (about 10–15 seconds) was small compared to the time between releases, during which the drift was assumed to occur. All further analysis was performed using this adjusted data, with no further experimental problems in the data becoming evident. The running average for the same probe with the adjusted data is shown in

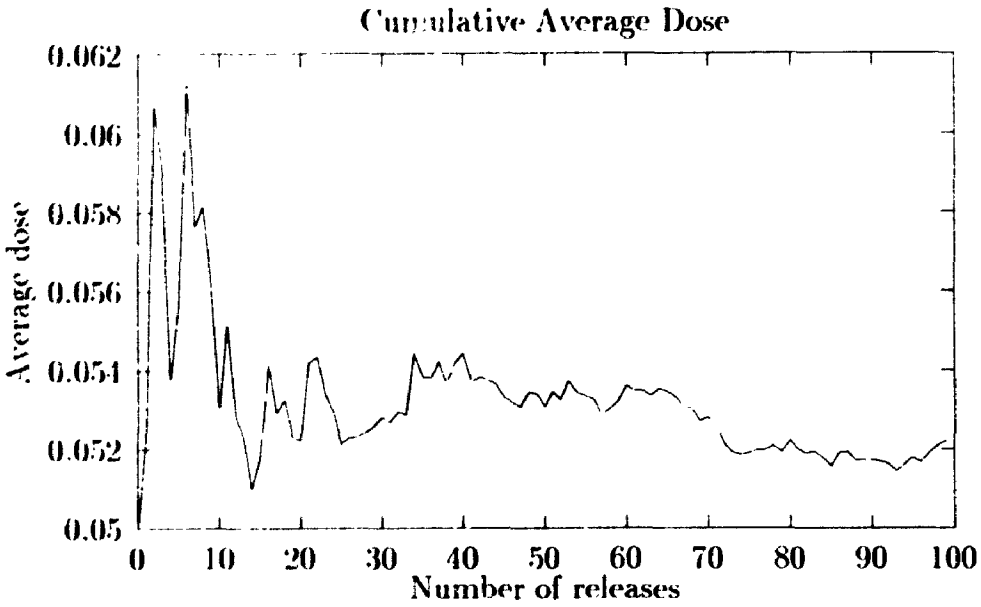

Figure 24: Same data as Figure (23) after drift adjustment.

Figure (24) repeated from Figure (7).

B.2 The $s - k$ Relationship

One observation which attracted interest was the inequality shown in Figures 20, 21 and 22 where $k > s^2 + 1$, for all data points. Investigation showed this to be a general relationship. Consider the integral

$$\int (x^2 + ax + b)^2 p(x)\, dx, \tag{61}$$

where p is any probability density function. Assume without loss of generality that the mean of p is zero, and the standard deviation is one. Then

$$\int x^3 p(x)\, dx = s \tag{62}$$

$$\int x^4 p(x)\, dx = k \tag{63}$$

where s is the skewness and k is the kurtosis. Then determine the values of a and b for which this integral is a minimum by taking the derivatives with respect to a and

b, setting them to zero, and solving for a and b. The equations for a and b are

$$\int x(x^2 + ax + b)\, p(x)\, dx = s + a = 0 \tag{64}$$

$$\int (x^2 + ax + b)\, p(x)\, dx = 1 + b = 0. \tag{65}$$

These may be solved directly to give $a = -s$ and $b = -1$, and thus

$$\int (x^2 + ax + b)^2\, p(x)\, dx \geq k - s^2 - 1 \geq 0, \tag{66}$$

since the integrand is positive or zero. The function $x^2 + ax + b$ can have at most two zeros, so the integral will be strictly positive unless $p(x)$ consists of two delta functions, located at the zeros of $x^2 + ax + b$.

Note in conclusion that this relationship corresponds to the requirement that the variance, expressed as the difference of the second moment and the square of the first moment, must be positive. The one case not covered, where the standard deviation σ is zero, corresponds to a single delta function probability distribution, just as $k - s^2 - 1 = 0$ corresponds to two delta functions if $\sigma \neq 0$.

Bibliography

[Bat49] G.K. Batchelor. Diffusion in a field of homogeneous turbulence—Eulerian analysis. *Australian Journal of Scientific Research*, A2:437–450, 1949.

[Bat51] G.K. Batchelor. Diffusion in a field of homogeneous turbulence—relative motion of particles. *Proceedings of the Cambridge Philosophical Society*, pages 48 345, September 1951.

[Bat64] G.K. Batchelor. Diffusion from sources in a turbulent boundary layer. *Archiwum Mechaniki Stosowanej*, 16:661–670, 1964.

[BBDT78] A.D. Birch, D.R. Brown, M.G. Dodson, and J.R. Thomas. Studies of flammability in turbulent flows using laser raman spectroscopy. Technical Report MRS E 348, British Gas Corporation, Midlands Research Station, August 1978.

[BC92] W.D. Baines and A.F. Corriveau. Mixing in turbulent jets as revealed by pH indicator. In *Proceedings of the 2nd Carribean Conference on Fluid Dynamics*, pages 142 148, St. Augustine, Trinidad, 1992.

[CAZ90] C. Contini, A. Amendola, and I. Ziomas. Uncertainties in chemical risk assessment as a result of a European benchmark exercise. In *Environmetrics: Second International Conference on Statistical Methods for the Environmental Sciences*, pages 48–50, Como, Italy, September 1990. Program and Abstracts.

[CC85] K.K. Carn and P.C. Chatwin. Variability and heavy gas dispersion. *Journal of Hazardous Materials*, 11:281 300, 1985.

[Cha90] P.C. Chatwin. Statistical methods for assessing hazards due to dispersing gases. *Environmetrics*, 1(2):143 162, 1990.

[CS77] P.C. Chatwin and P.J. Sullivan. Experiments on the complete mixing of passive contaminant in turbulent diffusion. In G.K. Patterson and J.L. Zakini, editors, *Proceedings of the 5th Biennial Symposium on Turbulence*, pages 211 216, Princeton, 1977. Science Press. Rolla, Miss.

[CS79] P.C. Chatwin and P.J. Sullivan. The relative diffusion of a cloud of passive contaminant in incompressible turbulent flow. *Journal of Fluid Mechanics*, 91:337 355, 1979.

[CS87] P.C. Chatwin and P.J. Sullivan. Perceived and statistical properties of scalars in turbulent shear flows. In *6th Symposium on Turbulent Shear Flows*, Toulouse, France, September 1987.

[CS89] P.C. Chatwin and P.J. Sullivan. The intermittency factor of scalars in turbulence. *Physics of Fluids A*, 4:761 763, 1989.

[CS90a] P.C. Chatwin and P.J. Sullivan. Cloud averaged concentration statistics. *Mathematics and Computers in Simulation*, 32:49 57, 1990.

[CS90b] P.C. Chatwin and P.J. Sullivan. A simple and unifying physical interpretation of scalar fluctuation measurements from many turbulent shear flows. *Journal of Fluid Mechanics*, 212:533 556, 1990.

[CS93] P.C. Chatwin and P.S. Sullivan. The structure and magnitude of concentration fluctuations. *Boundary Layer Meteorology*, 62:269 280, 1993.

[DS87] R.W. Derksen and P.J. Sullivan. Deriving contaminant concentration fluctuations from time-averaged records. *Atmospheric Environment*, 21:597 608, 1987.

[DS90] R.W. Derksen and P.J. Sullivan. Moment approximations for probability density functions. *Combustion and Flame*, 81:378–391, 1990.

[DSB91] W.J. Dahm, K.B. Southerland, and K.A. Buch. Direct, high resolution, four dimensional measurements of the fine scale structure of $Sc \gg 1$ molecular mixing in turbulent flows. *Physics of Fluids A3*, 5:1115–1127, 1991.

[DSY94] R.W. Derksen, P.J. Sullivan, and H. Yip. Asymptotic probability density function of a scalar. *AIAA Journal*, 31:1083–1084, 1994.

[DT92] H.H. Dayal and N. Trieff. Mathematical models in exposure assessment from a chemical spill. In *The 4th International Conference on Statistical Methods for the Environmental Sciences*, pages 101–102, Espoo, Finland, August 1992. Helsinki University of Technology.

[FR82] J.E. Fackrell and A.G. Robins. Concentration fluctuations and fluxes in plumes from point sources in a turbulent boundary layer. *Journal of Fluid Mechanics*, 117:1 26, 1982.

[Gri91] R.F. Griffiths. The use of probit expressions in the assessment of acute population impact of toxic releases. *Journal of Loss Prevention in the Process Industries*, 4:49- 57, 1991.

[HWM+91] D.J. Hall, R.A. Waters, G.W. Marsland, S.L. Upton, and M.A. Emmott. Repeat variability in instantaneously released heavy gas clouds - some wind tunnel model experiments. Report LR 804, Warren Spring Laboratory, (PA)Department of Trade and Industry, U.K., 1991.

[Kaw93] G. Kawal. Private Communication. 1993. Department of Mechanical Engineering, University of Toronto, Toronto, Canada.

[LC94] D.M. Lewis and P.C. Chatwin. The treatment of atmospheric dispersion data in the presence of noise and baseline drift. *Boundary-Layer Meteorology*, 1994. To appear.

[LS94] F. Labropulu and P.J. Sullivan. The prediction of the probability density function of contaminant concentration in turbulent flows. In *Eleventh Canadian Symposium on Fluid Dynamics*, pages 36–37, Edmonton, Canada, June 1994. University of Alberta.

[LSY94] F. Labropulu, P.J Sullivan, and H. Ye. A model of near-source turbulent mixing. *Transactions of the Canadian Society of Mechanical Engineers*, 1994. In press.

[MC94] N. Mole and E. D. Clarke. Simple extensions to the Chatwin and Sullivan theory. *Boundary Layer Meteorology*, 1994. In press.

[MCS93] N. Mole, P.C. Chatwin, and P.J. Sullivan. Modelling concentration fluctuations in air pollution. In B. Beck, M. McAleer, and A.J. Jakeman, editors, *Modelling Change in Environmental Systems*, pages 317–340. John Wiley & Sons Ltd., 1993.

[Mos91] D. J. Moseley. A closure hypothesis for contaminant fluctuations in turbulent flow. Master's thesis, The University of Western Ontario, London, Ontario, April 1991.

[MY71] A.S. Monin and A.M. Yaglom. *Statistical Fluid Mechanics: Mechanics of Turbulence*, volume 1. The MIT Press, Cambridge, Massachusetts, and London, England, 1971.

[PHC93] M. Poreh, A. Hadad, and J. Cermak. Fluctuations of line integrated concentrations across plume diffusion in grid generated turbulence and in shear flows. *Boundary-Layer Meteorology*, 62:247-267, 1993.

[SHRJ92] M. Sandberg, S. Hellberg, S. Rännar, and J Jonsson. Models for prediction of human toxicity: Multivariate validation of cell toxicity data. In *The 4th International Conference on Statistical Methods for the Environmental Sciences*, pages 39–40, Espoo, Finland, August 1992. Helsinki University of Technology.

[SS94] B.L. Sawford and P.J. Sullivan. A simple representation of a developing contaminant concentration field. *Journal of Fluid Mechanics*, 1994. Submitted.

[Sul84] P.J. Sullivan. Whence the fluctuations in measured values of mean-square fluctuations? In G.A. Beals and N.E. Bowne, editors, *Proceedings of the 4th Joint Conference on Applications of Air Pollution Meteorology*, pages 115 121, 1984.

[Sul90] P.J. Sullivan. Physical modeling of contaminant diffusion in environmental flows. *Environmetrics*, 1(2):163–177, 1990.

[SY91] P.J. Sullivan and H. Yip. Contaminant dispersion from an elevated point source. *ZAMP*, 42:315–318, 1991.

[SY93] P.J. Sullivan and H. Ye. Further comments on "cloud-averaged" concentration statistics. *Mathematics and Computers in Simulation*, 35:263–269, 1993.

[SY94] P.J. Sullivan and H. Ye. A moment description of the probability density function for contaminant concentration values in turbulent flows. In

Eleventh Canadian Symposium on Fluid Dynamics, pages 36–37, Edmonton, Canada, June 1994. University of Alberta.

[TL72] H. Tennekes and J.L. Lumley. *A First Course in Turbulence*. The MIT Press, Cambridge, Massachusetts, and London, England, 1972.

[War84] Z. Warhaft. The interference of thermal fields from line sources in grid turbulence. *Journal of Fluid Mechanics*, 144:363–387, 1984.